EMC Conducted Emissions Test

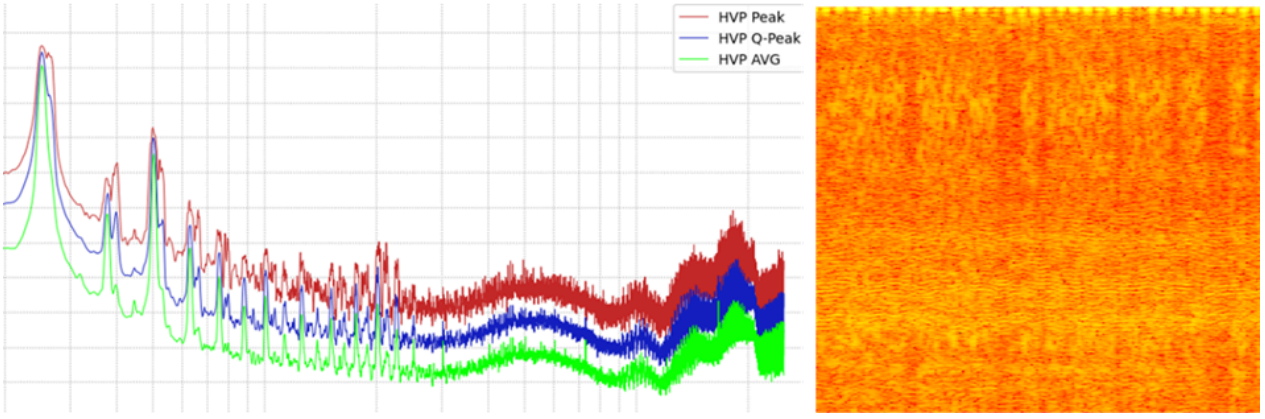


Table of contents

- Introducition
- Test setup
- EMI Filter Schematic Reminder
- Common-mode and Differential-mode Separation
- HVP HVN, Vin 380V, Before using input filter
  - HVP & HVN Q-Peak
  - HVP Q-Peak, Peak and AVG
  - HVN Q-Peak, Peak and AVG
- Common Mode Choke (CMC) impact
- Adding film capacitors and snubber
- Adding ceramic y-capacitors
- Try differential snubber 220nF and 2.4 ohm
- Try common mode snubber 4.7nF and 360 ohm
- EMC measurement with and without EMI filter
  - HVP and HVN Q-Peak after using the EMI filter
  - HVP Q-Peak, Peak and AVG, after using EMI filter
  - HVN Q-Peak, Peak and AVG, after using EMI filter
  - HVP Q-PEAK before vs after using EMI filter
- Other investigation
  - Frequency sweep (spread spectrum)
  - Impact of 220 nF capa in diff mode on the LISN side
  - Impact of 1.5 µF capa in diff mode on the LISN side
  - Impact of 100nF capa in common mode on the switchs side
  - Analysis of the significant effect of differential capacitors 220 nF and 1.5 µF
- Annexes
  - Main power supply noise
  - FlyBack noise
  - EMI impact of Gate driver resistor (Rg)
  - Common-mode and Differential-mode Separation (Math)

Introducition

The goal of this test is to see the impact of the EMI filter on the conducted emissions of the DC-DC converter.
Since we don't have a professional EMI receiver, the idea is to use an isolated oscilloscope powered by a 12V battery, and to use a Python package that we already developed and validated to emulate an EMC receiver.

For more details about this EMI emulator, you can see the PyPi page or the github page of this project.

The available oscilloscope for this test is the Tektronix TDS3034B, which has a limited memory depth of 10k points.
To have a longer signal, the idea is to perform many acquisitions using a Python script (for more details see **EMI_saving_1CH.py**). We chose a horizontal resolution of 20 µs/div, and with 10k points the sampling time is 20 ns (50 MS/s), giving a recorded duration of 200 µs per shot. We will perform 50 shots each time, resulting in a total measurement time of 10 ms.

No trigger is configured—each shot is taken randomly to avoid any bias in the measurement.

After each measurement, we use the Python EMI-receiver emulator to preprocess the signal and estimate AVG, PEAK, and QPEAK.

Limitations of this test

- No EMI receiver, but the oscilloscope coupled with Python code gives satisfying results.
- No conventional setup, but using a metallic ground plane and a 5 µH LISN approximates the standard setup.
- This test is not intended for absolute measurements (like comparing the results to standard limits). It is only intended to compare the “before” and “after” of each modification. Absolute measurements may not be very accurate, but we hope that the delta will be accurate enough.

Test setup

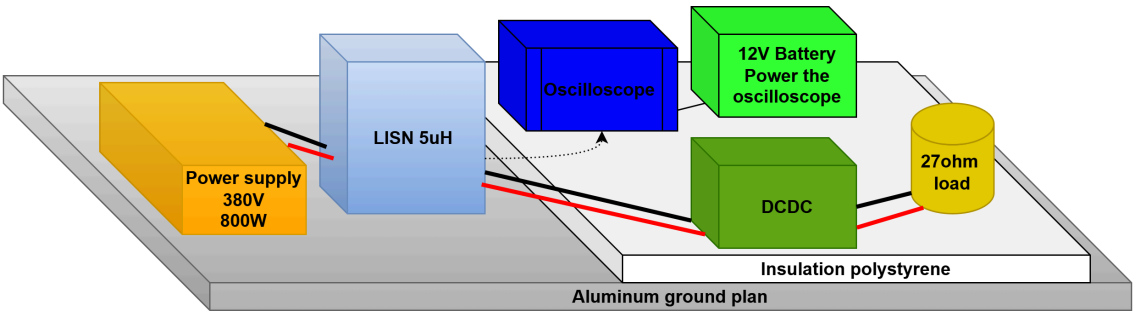


Figure 1: Setup schematic

The setup is composed of a power supply (345V–405V, 800W) fixed to 380V as the nominal voltage, a LISN of two phases of 5 µH, the DCDC converter, a secondary load of 27 Ω, the oscilloscope, and its battery to ensure isolation.

- The DCDC and the load are placed on top of an insulating polystyrene layer of around 2 cm. The output voltage is regulated to 42V. We chose a low voltage to avoid under-resonance issues since the current software is not the final version. With this configuration, we will have around 70 W at the output, which is enough to observe the DCDC noise.
- The DCDC is placed on top of two fans powered by its internal flyback, and it is grounded to the aluminum plane using two ground braids.
- The LISN is also grounded to the aluminum plane using its ground braid.
- The oscilloscope is isolated using several polystyrene layers to minimize the parasitic capacitance.
- The load and all wires are placed in the top of the polystyrene layer to reduce the parasite capacitor with ground

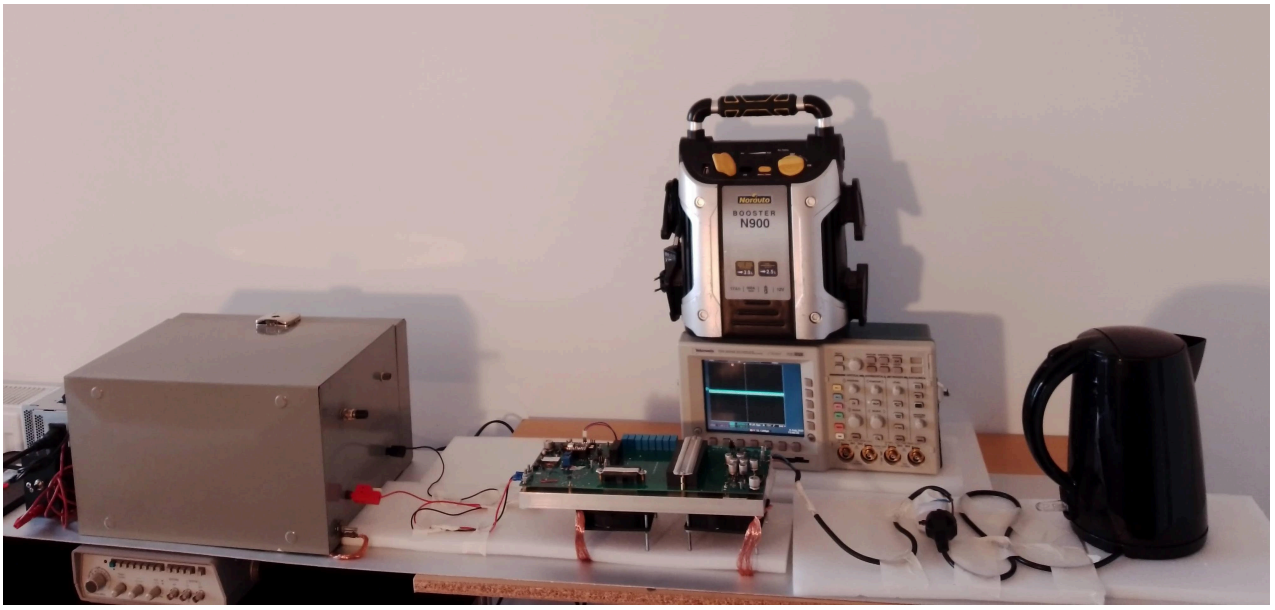


Figure 2: full setup



Figure 3: full setup, load

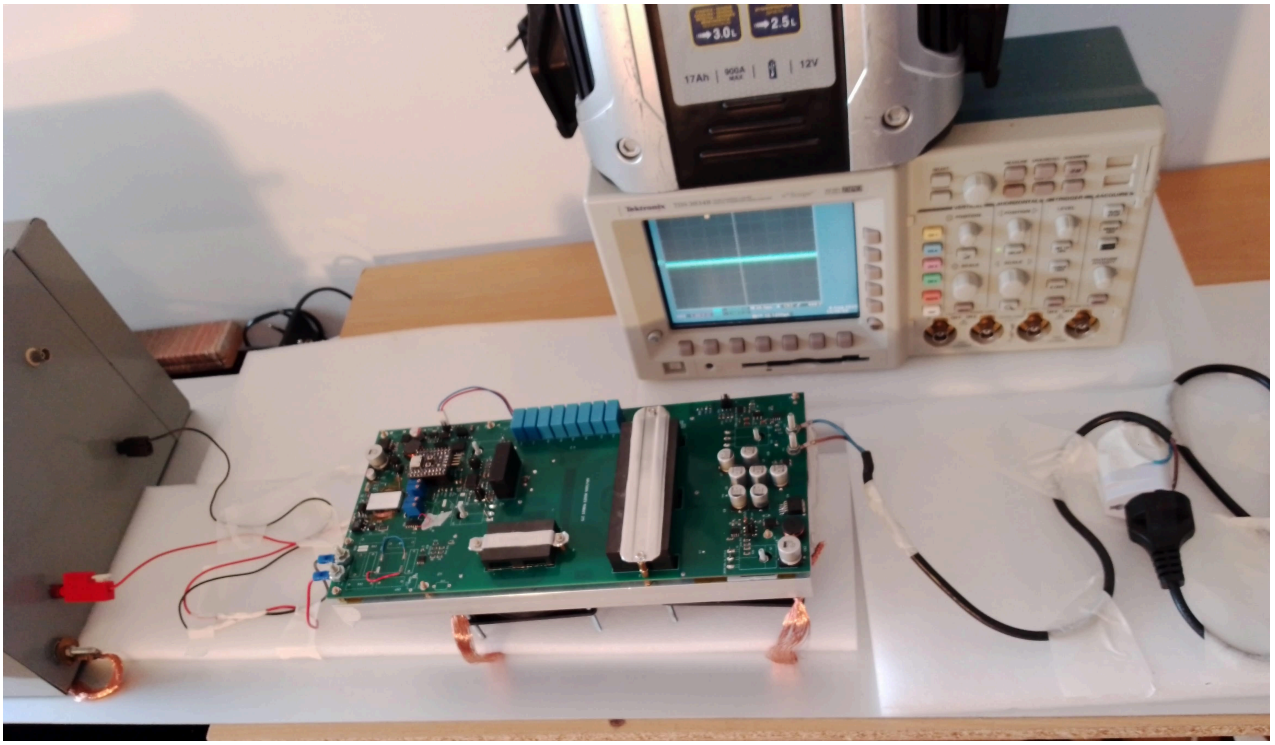


Figure 4: grounds of the dcdc and the LISN

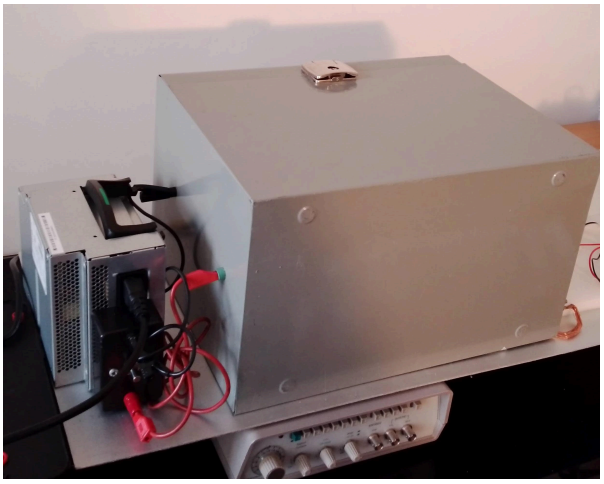


Figure 5: LISN and power supply

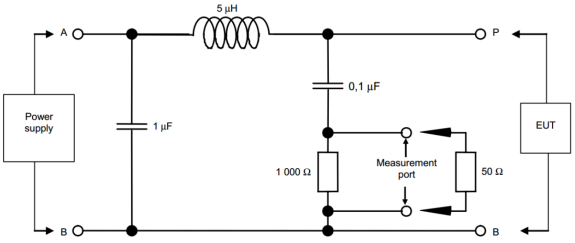


Figure 6: 5µH LISN schematic

EMI Filter Schematic Reminder

Below is a reminder of the proposed schematic of the EMI filter.
The snubber capacitor is changed from 2.2nF to 15nF.

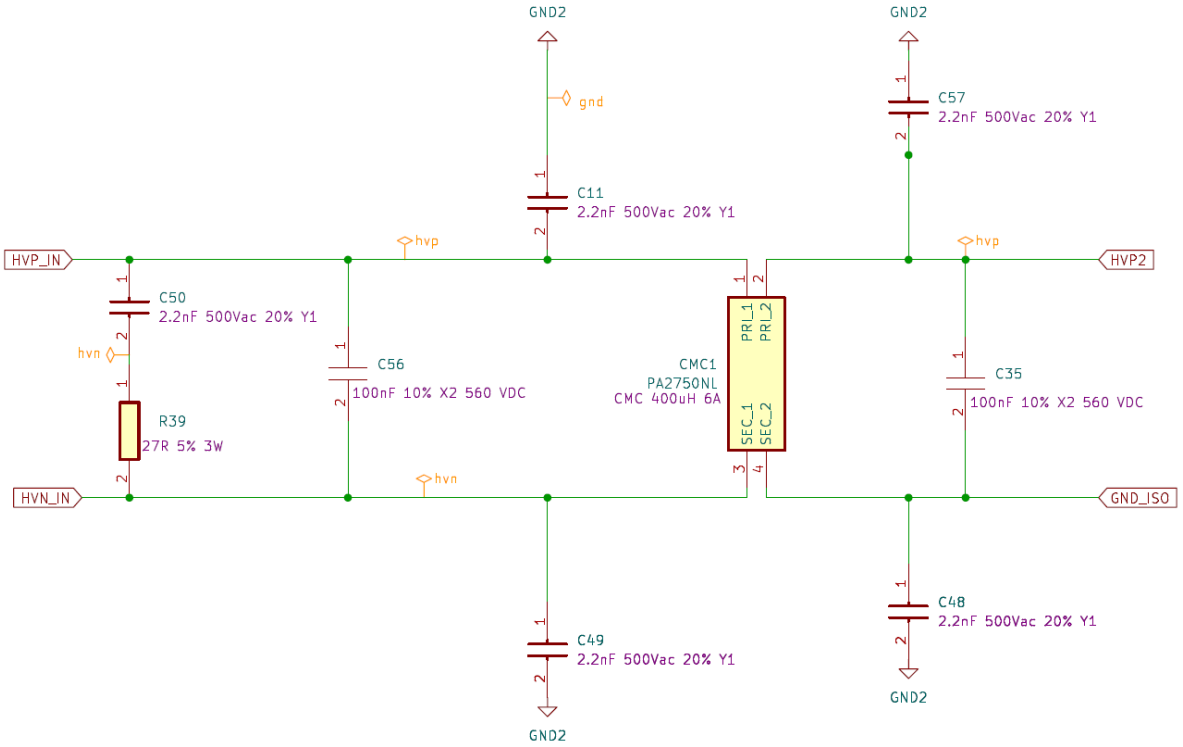


Figure 7: The main EMI filter schematic

Below the position of the 5 ceramic-y capacitors.
The ceramic capacitor used is 400VAC 102M 1NF (1nF) instead of 220pF as you can see below.

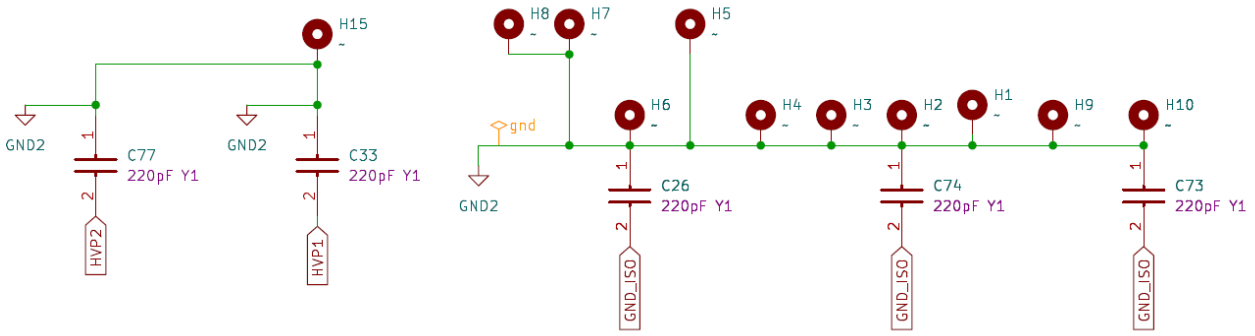


Figure 8: Ceramic y-caps 1nF

Common-mode and Differential-mode Separation

In all tests, we try to separate the common-mode noise from the differential-mode noise. To do this, we use a magnetic core recovered from a failed Tektronix TCP1015 current probe.
We added five external turns to form a secondary winding, and this secondary is connected to the oscilloscope using its 50-ohm internal termination.

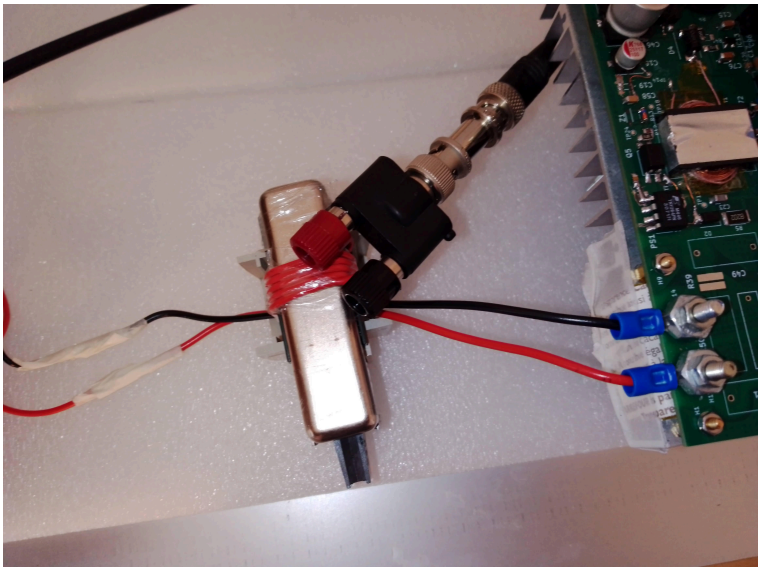


Figure 9: Magnetic core of TCP0150 (common mode)

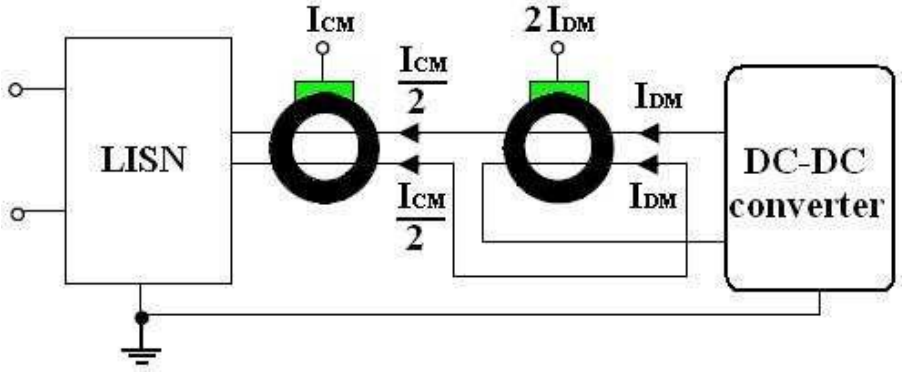


Figure 10: Common mode and differential mode measurement method

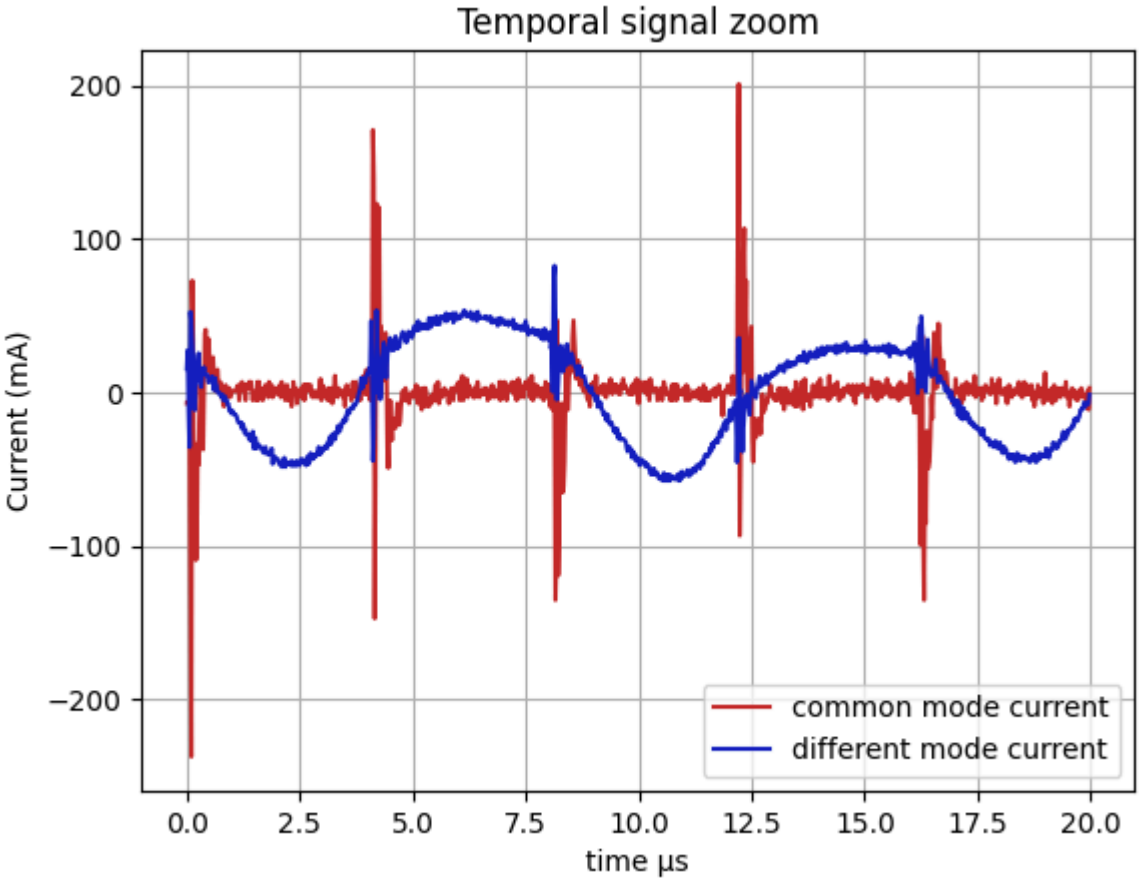
Below are the formulas used to convert the measured voltage into the estimated common-mode and differential-mode currents.

$$i_{cm} = \left(\left(\frac{\text{Channel}_{Voltage}}{R_{Terminal}} \right) \cdot \text{Nturns} \right)$$

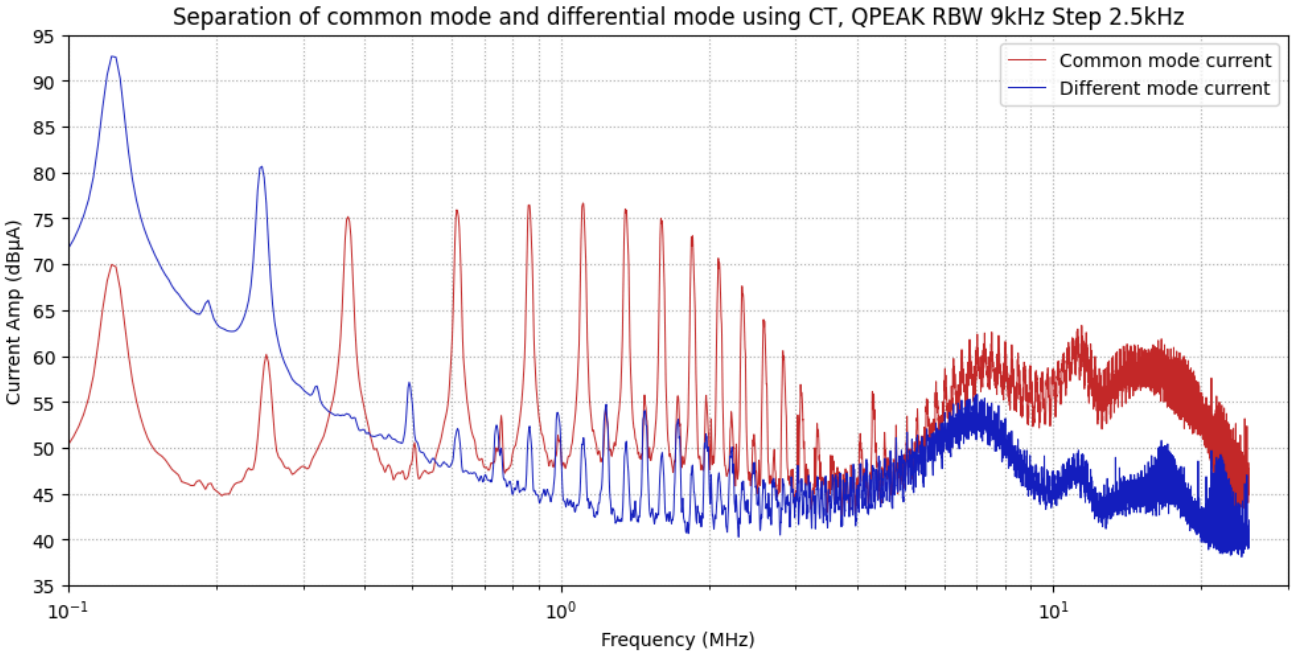
$$i_{dm} = \frac{\left(\frac{\text{Channel}_{Voltage}}{R_{Terminal}} \right) \cdot \text{Nturns}}{2}$$

A zoom plot of both estimated currents

```
Text(0, 0.5, 'Current (mA)')
```



Below is the QPEAK estimation of both currents. We can see that the **differential-mode current is predominant at low frequency (up to around 300 kHz)**, while the **common-mode current becomes predominant above this frequency**.



Below is an estimation of the reflected resistor using this setup. We can see that **2 Ω is a high value**, so using the oscilloscope's **50 Ω input** as the load of the current transformer is a bad idea. Next time, we must add a **low external load**, such as **1 Ω**, so the reflected resistance on the primary will be only **40 mΩ**.

$$R_{Terminal} = 50 \ \ (\Omega)$$

$$N_{turns} = 5$$

$$R_{reflected} = \frac{R_{Terminal}}{(N_{turns})^2} = \frac{50}{(5)^2} \qquad = 2.000 \ \ (\Omega)$$

HVP HVN, Vin 380V, Before using input filter

In this test, we will measure the DCDC conducted emissions without a filter; this will be our reference to evaluate the filter's impact.

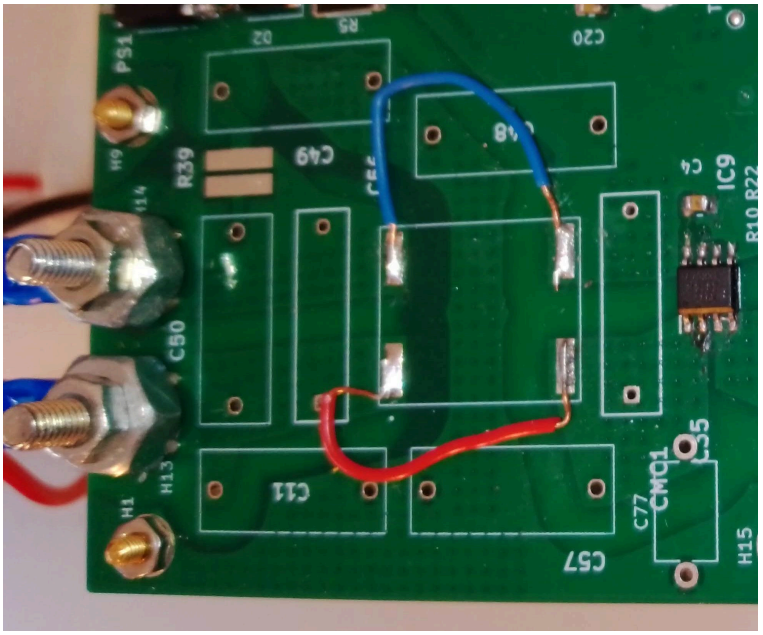
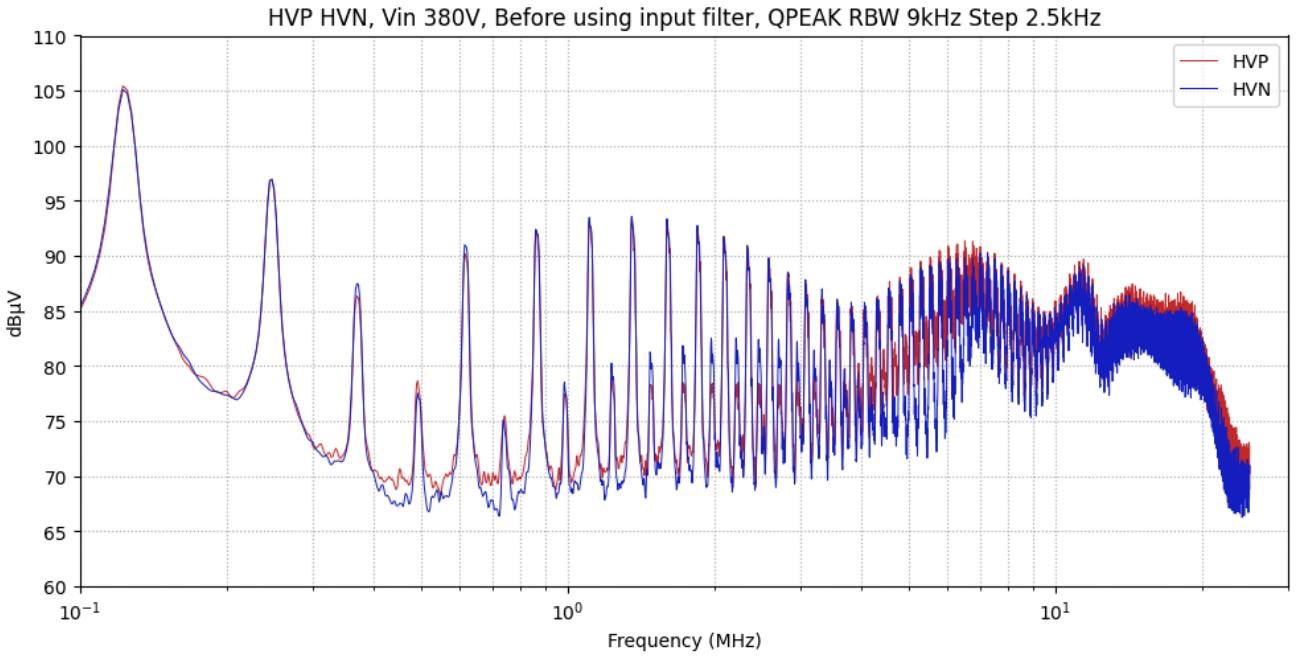
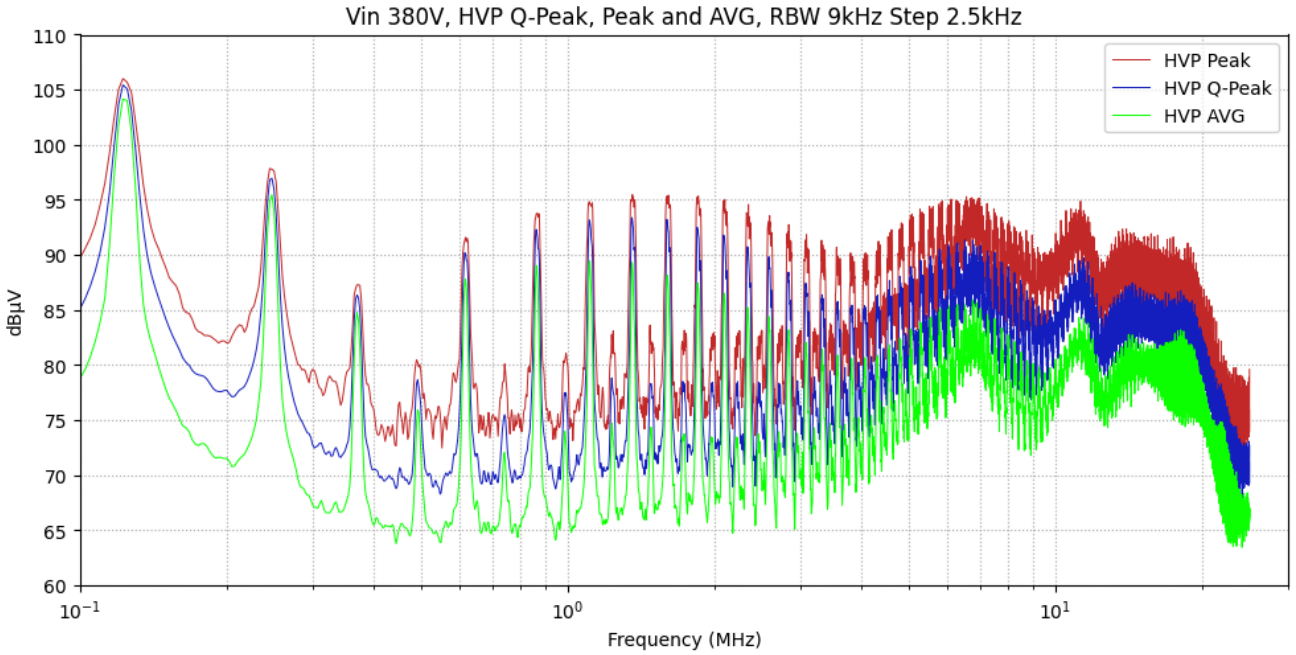


Figure 11: PCB: Input filter zone

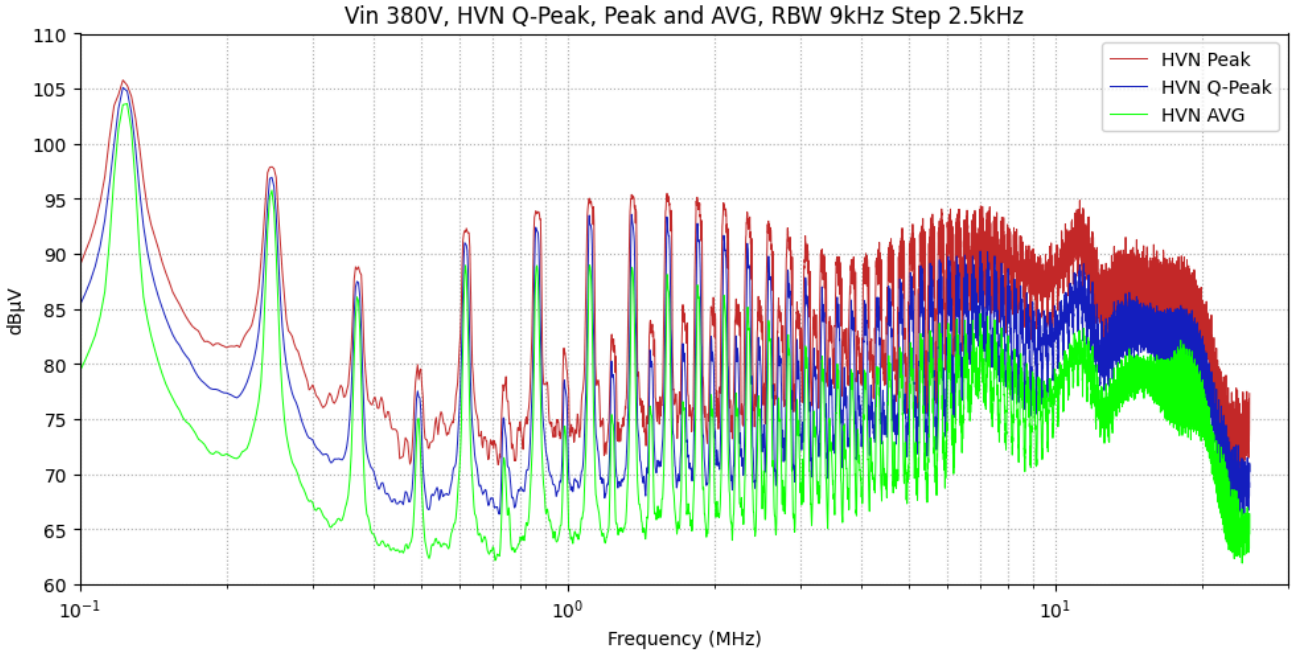
HVP & HVN Q-Peak



HVP Q-Peak, Peak and AVG



HVN Q-Peak, Peak and AVG



Common Mode Choke (CMC) impact

Start by adding the common-mode choke (CMC) to the filter; no other elements are added. See the figures below.

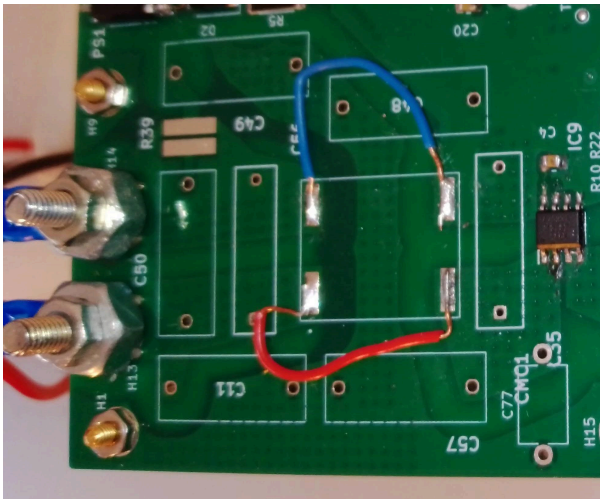


Figure 12: Before

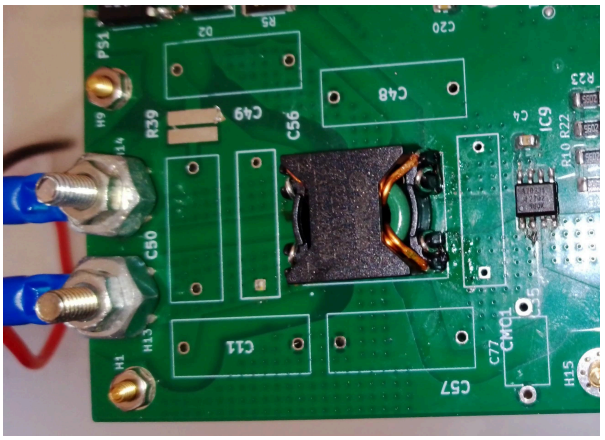
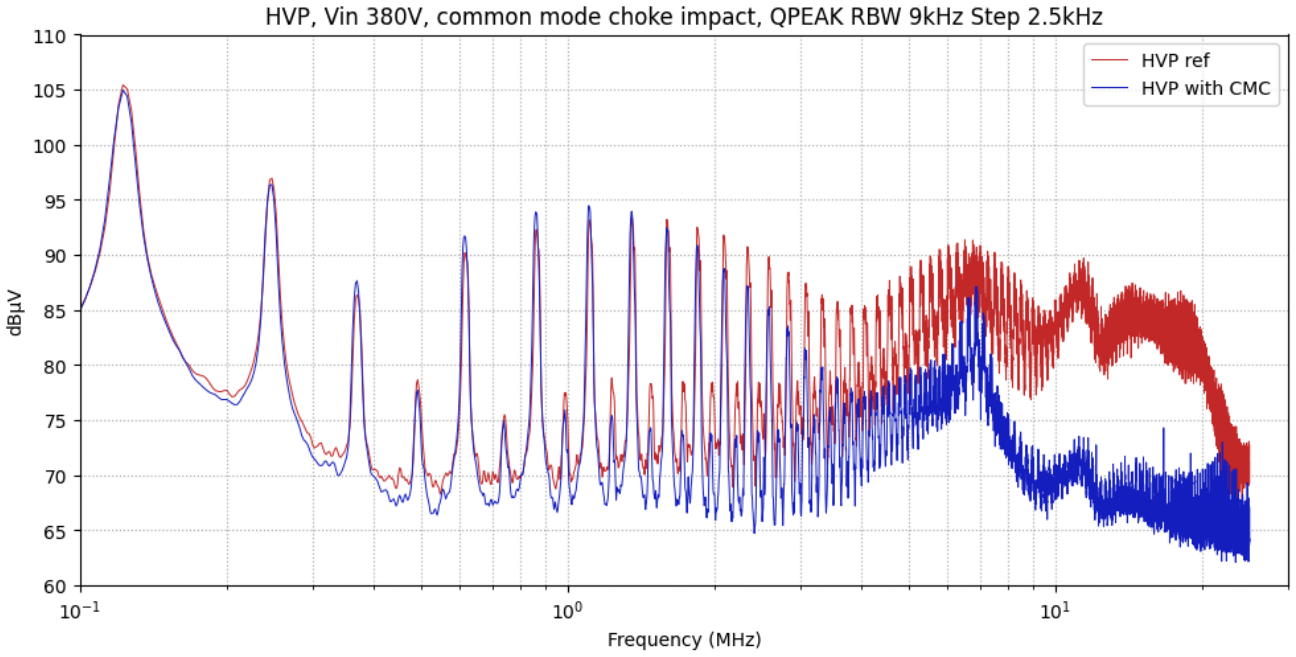


Figure 13: After



The CMC has a visible impact in the high frequencies starting from 2 MHz, but only a slight impact below this frequency.

Adding film capacitors and snubber

In this step, we will add another film capacitor and the differential snubber (15 nF + 27 Ω).

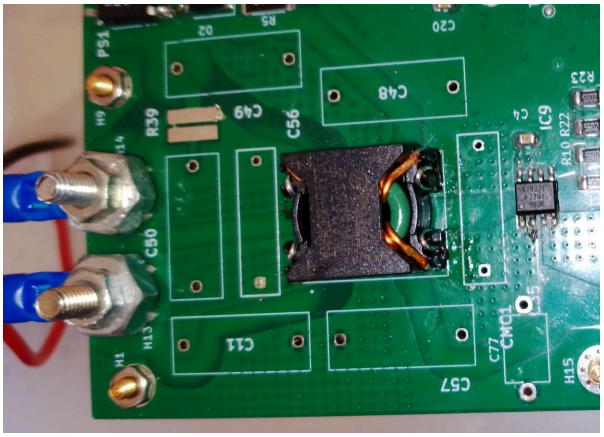


Figure 14: Before

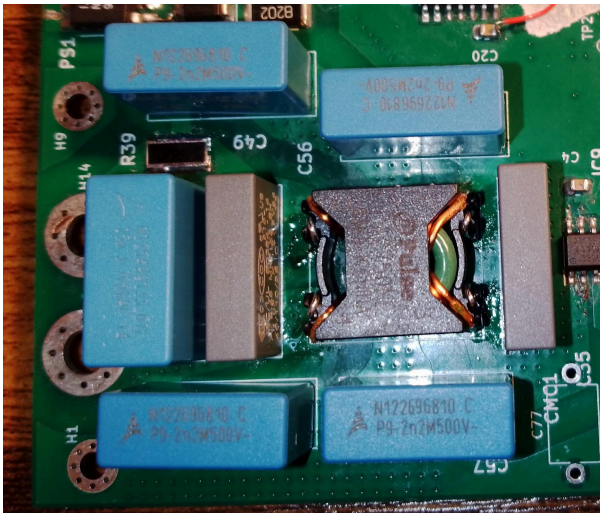
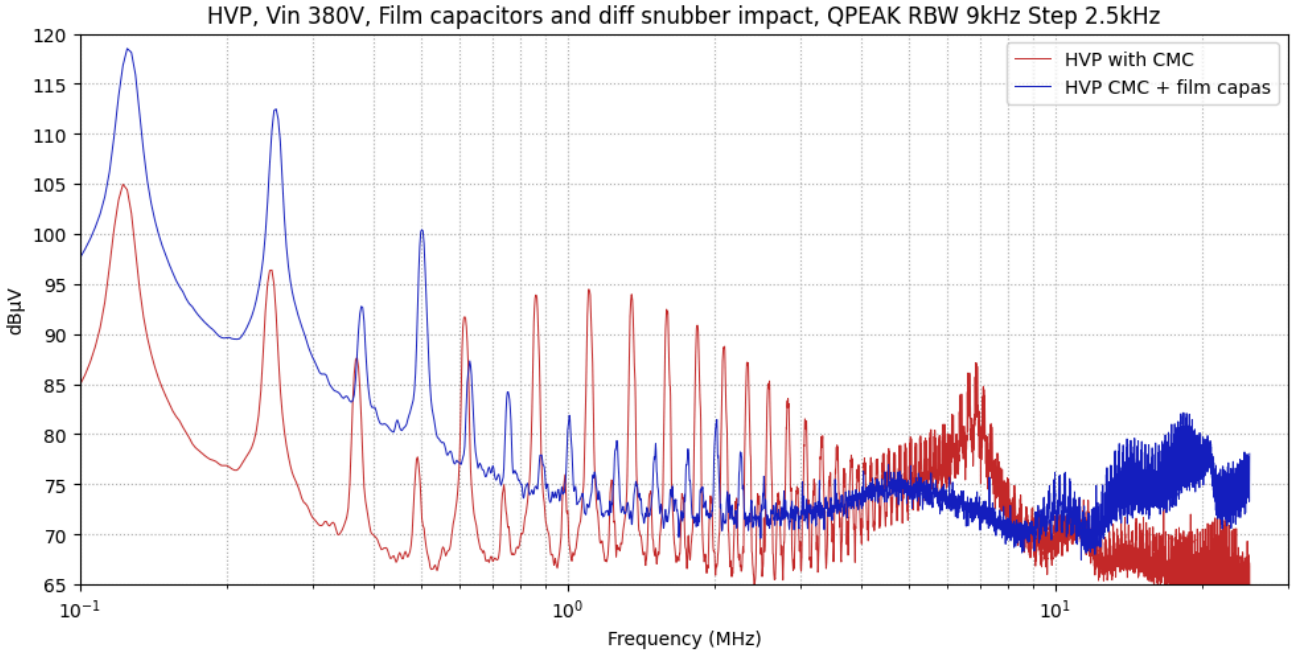


Figure 15: After



The film capacitors (common-mode and differential-mode) help the filter at high frequencies, starting from around 600 kHz, but they have a negative impact at low frequencies.

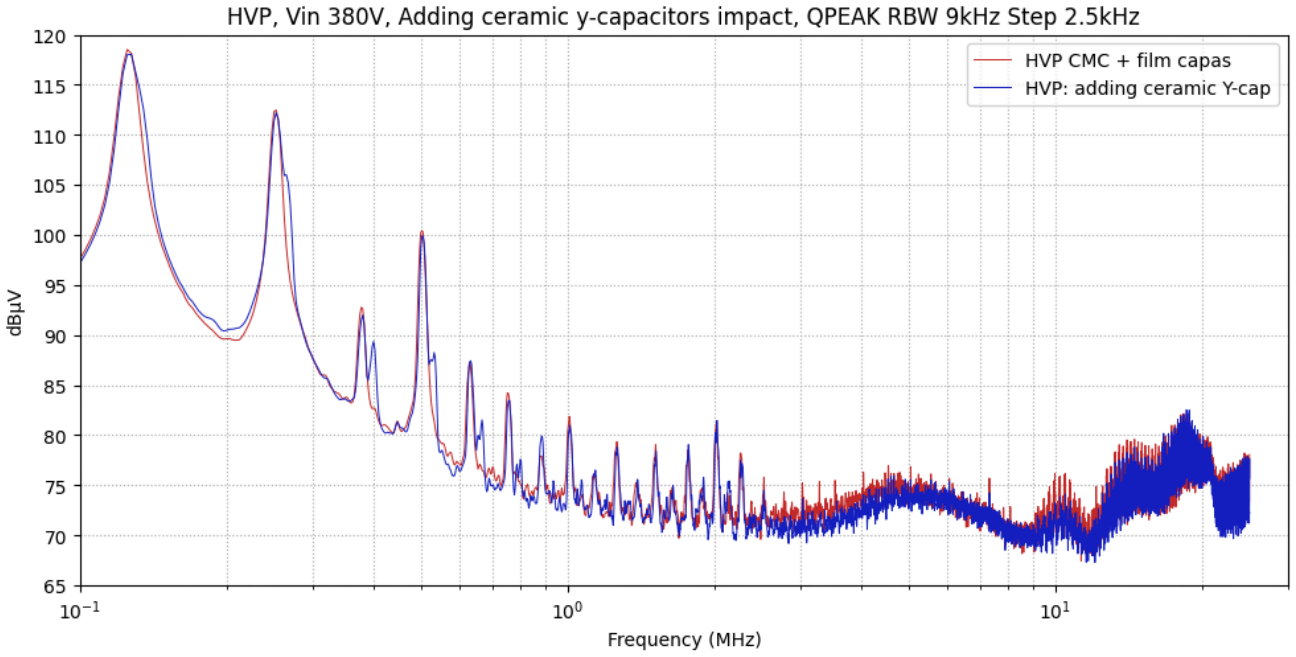
We must analyze by simulation whether there is a resonance with the LISN and the wiring impedance.

Adding ceramic y-capacitors

Since all control circuits are referenced to HVN, the five ceramic Y-capacitors connect this potential to ground at four different points, and an additional ceramic capacitor connects HVP to ground



Figure 16: The Y-ceramic capacitors are circled in red



We observe slight improvements in the high-frequency range (from around 2 MHz), but the effect is not very significant. We expect these capacitors to have more impact at higher frequencies.

Try differential snubber 220nF and 2.4 ohm

To investigate the performance degradation observed after adding the film capacitor, we added this differential snubber on the noise side to check whether it provides any low-frequency damping.

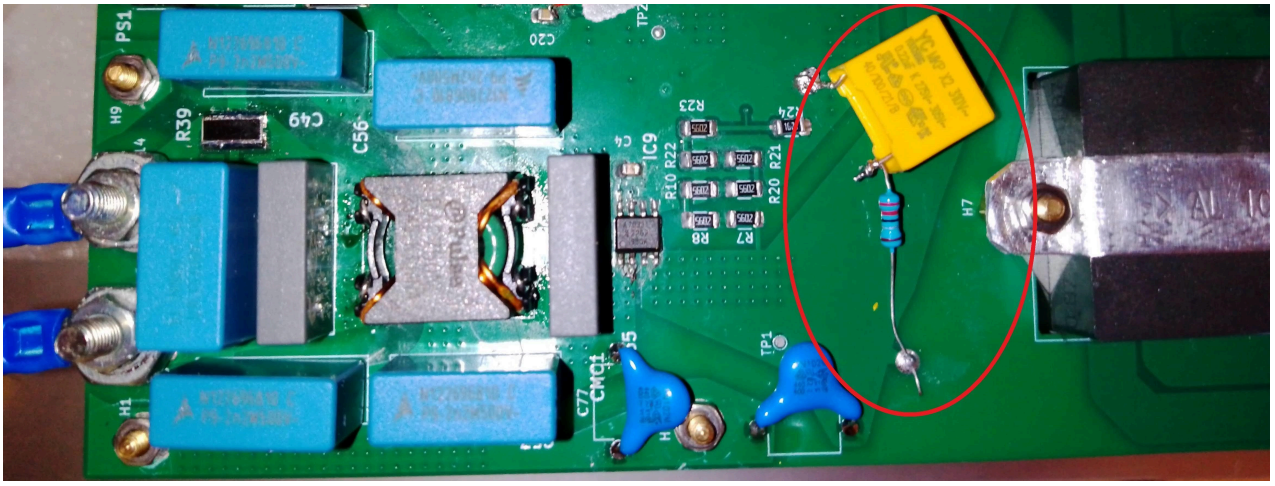
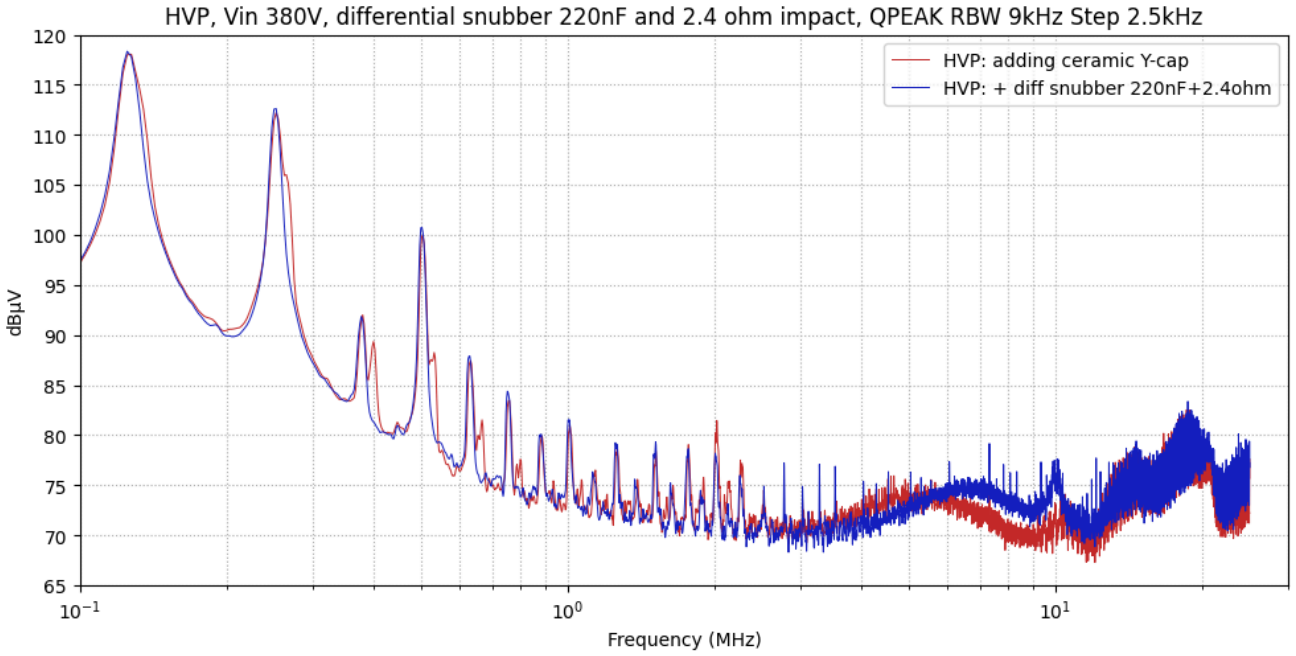


Figure 17: The prototype of a differential-mode snubber (0.22 µF & 2.4 Ω) is circled in red



There is almost no improvement, particularly in the low-frequency range. Only a slight effect is visible between 2 MHz and 10 MHz, suggesting that the issue is likely not caused by a differential-mode resonance

Try common mode snubber 4.7nF and 360 ohm

Based on the differential snubber results, we now add the common-mode snubber to determine whether the issue originates from a common-mode resonance.

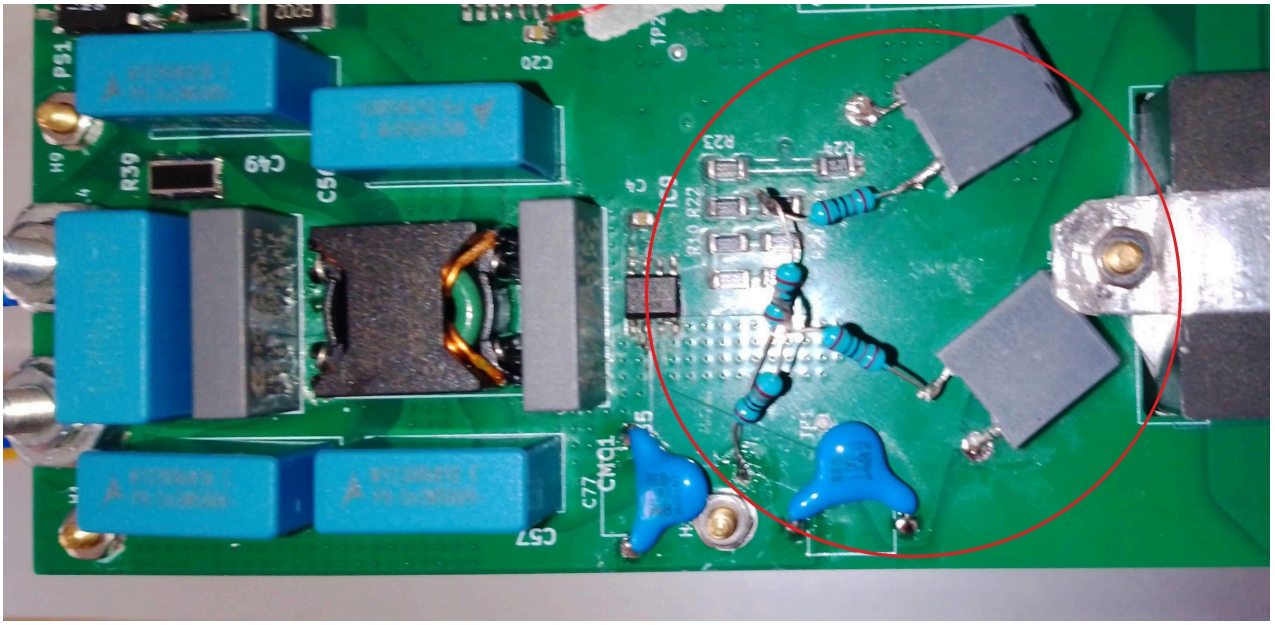
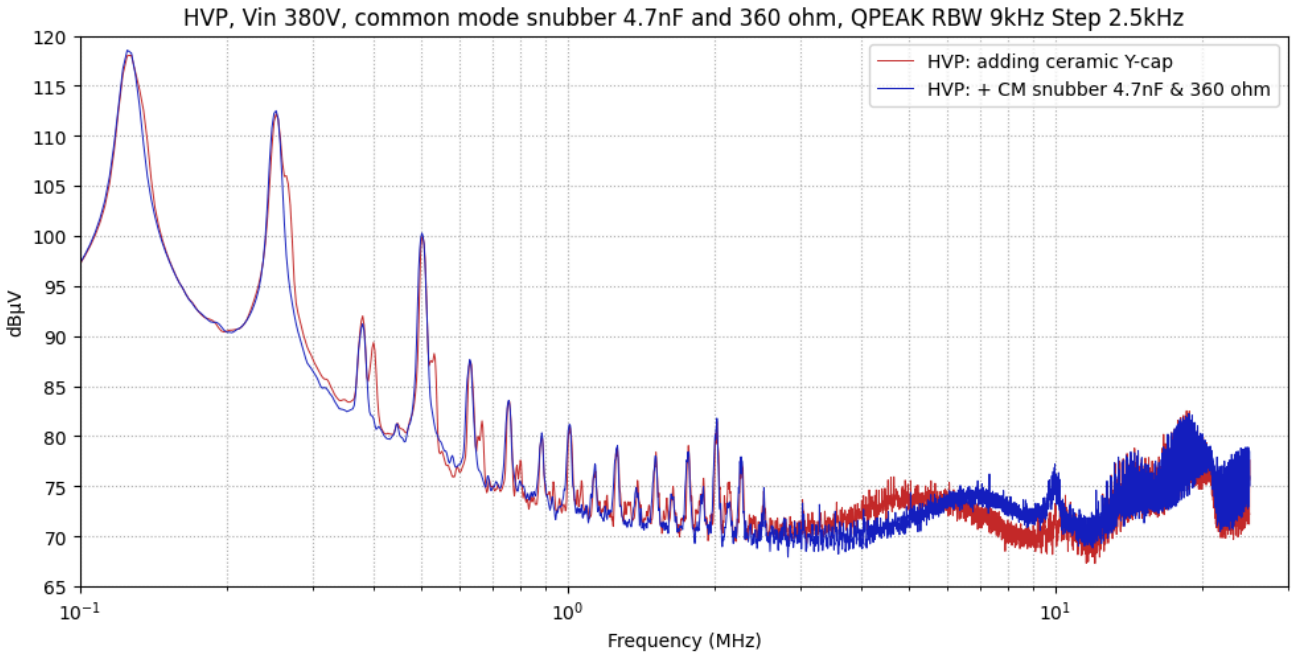


Figure 18: The prototype of a common-mode snubber (4.7 nF & 360 Ω) is circled in red

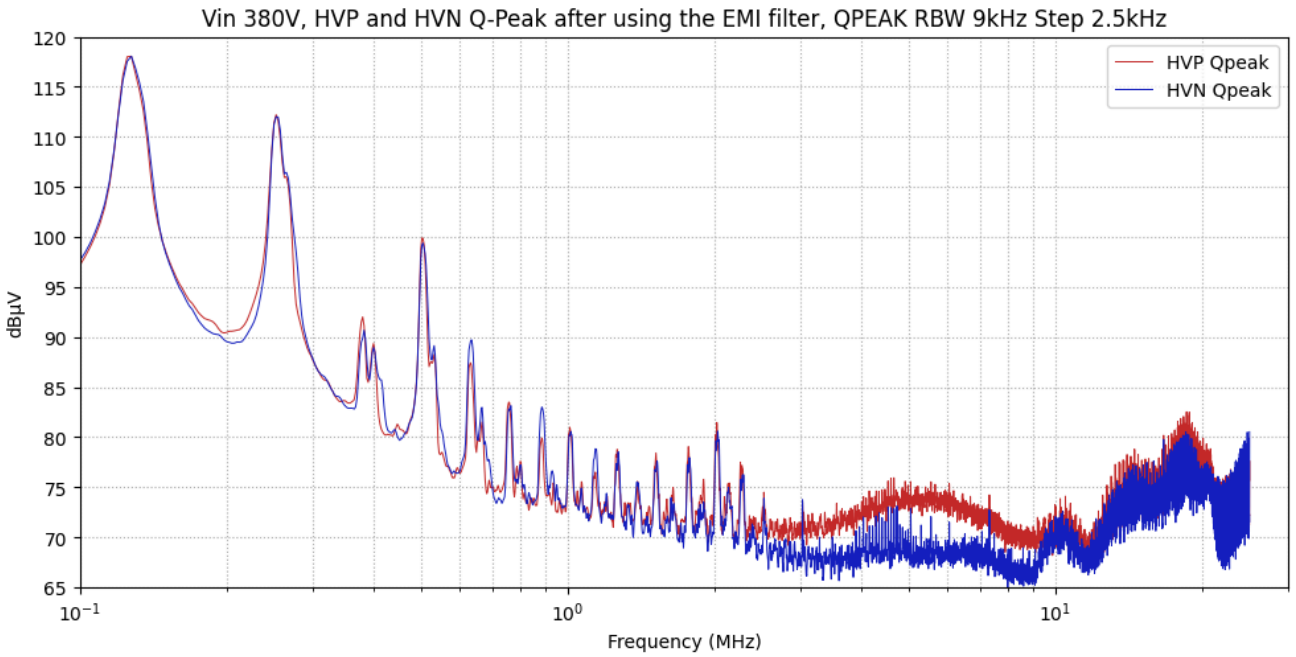


The behaviour is almost identical to the differential snubber. Further, more detailed investigation is required to understand the impact of the film capacitor at low frequencies.

EMC measurement with and without EMI filter

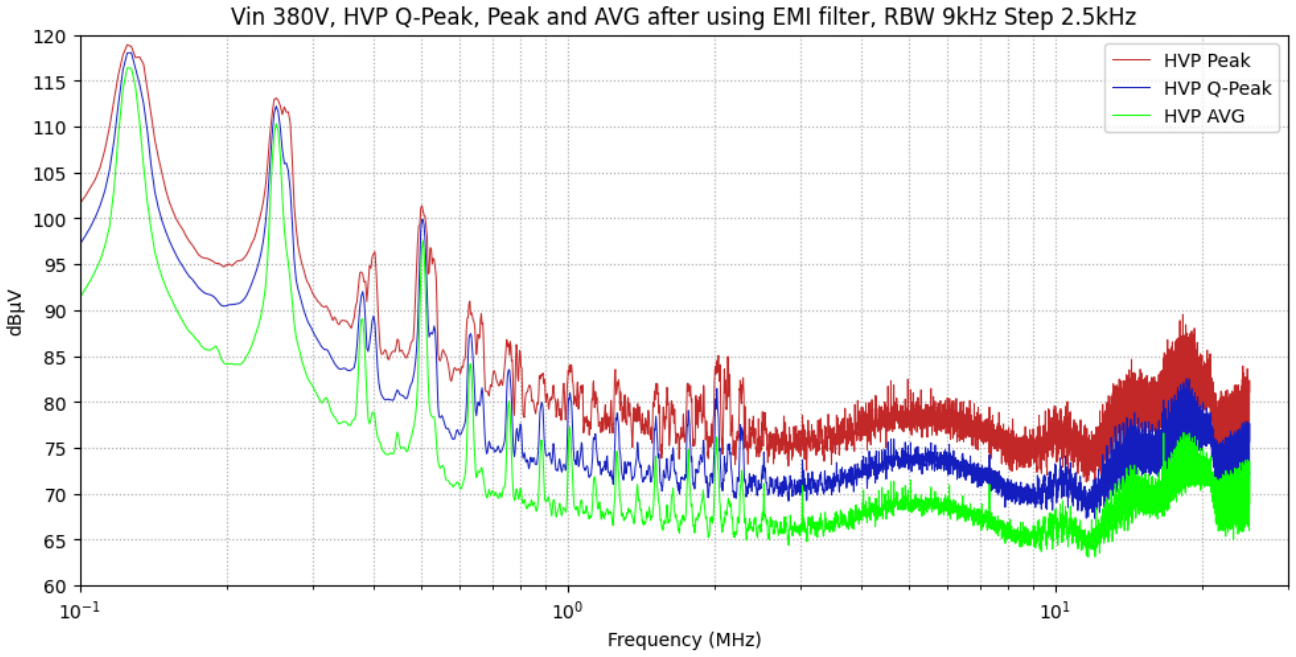
In this section, we simply compare the system performance before and after adding the EMI filter. All prototype snubbers have been removed, and only the original EMI filter configuration is retained.

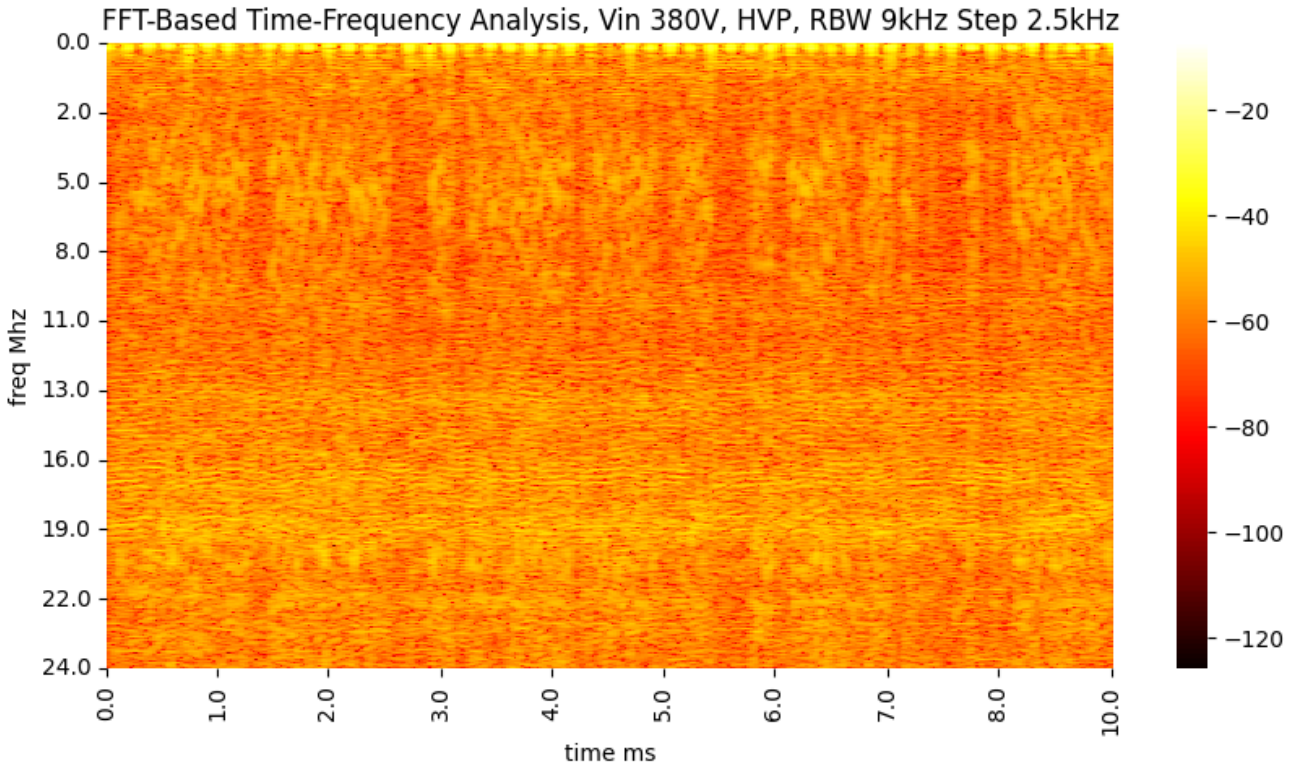
HVP and HVN Q-Peak after using the EMI filter



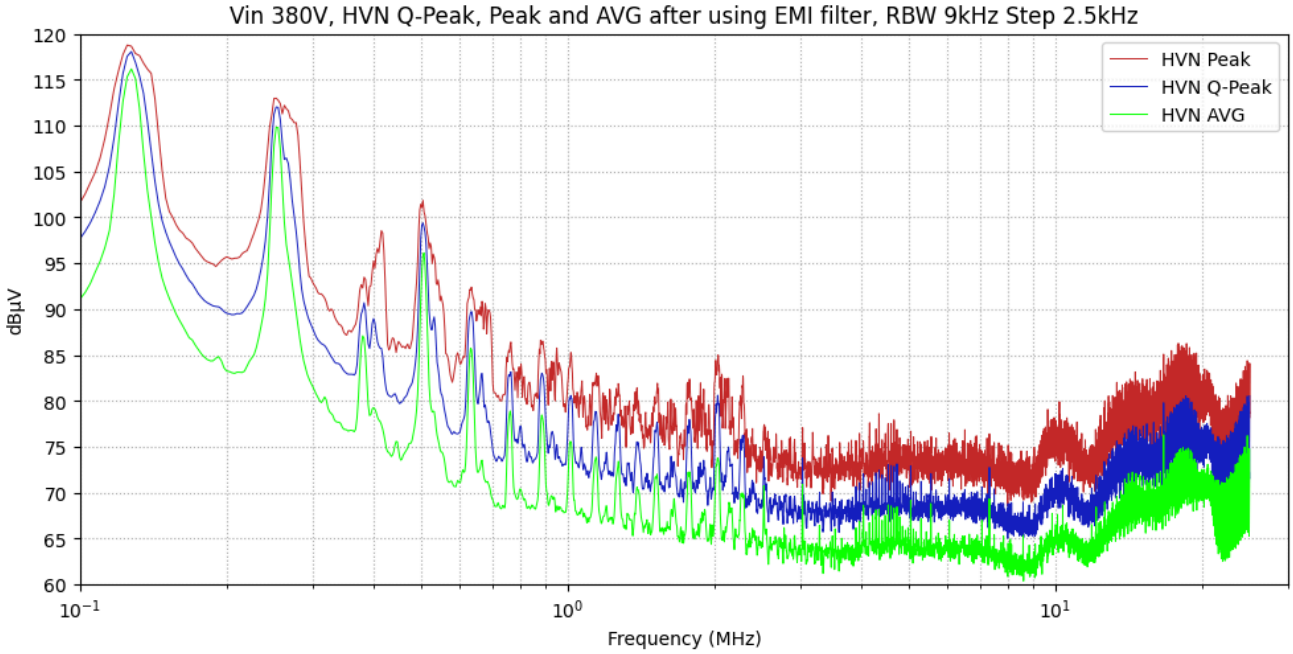
HVP and HVN show nearly identical behaviour, with a slight difference on HVP between 2 MHz and 20 MHz. This may be due to the asymmetry between the two HV poles: HVN serves as the control-circuit reference, while HVP ends at the drain of the high-side primary MOSFET.

HVP Q-Peak, Peak and AVG, after using EMI filter

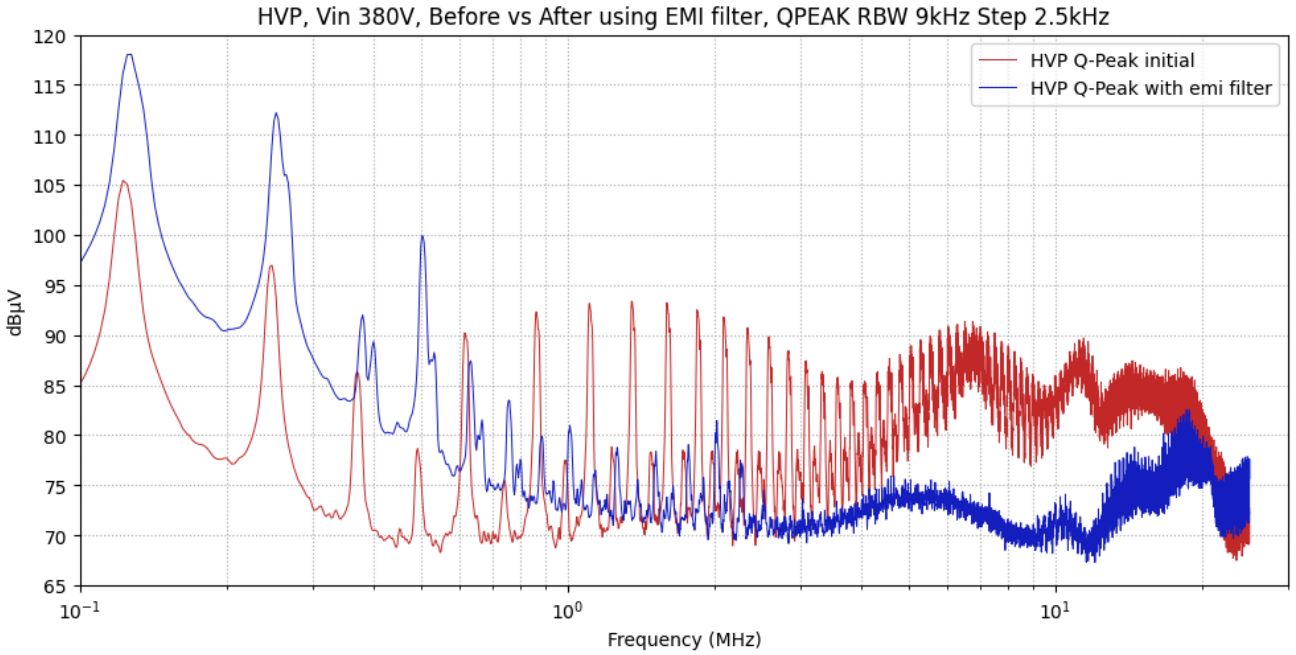




HVN Q-Peak, Peak and AVG, after using EMI filter



HVP Q-PEAK before vs after using EMI filter



The EMI filter provides effective attenuation at high frequencies, beginning around 600 kHz, but it degrades performance at lower frequencies.
This filter version is a solid starting point; however, additional simulations, analysis, and testing are required to improve the performance, particularly in the low-frequency range.

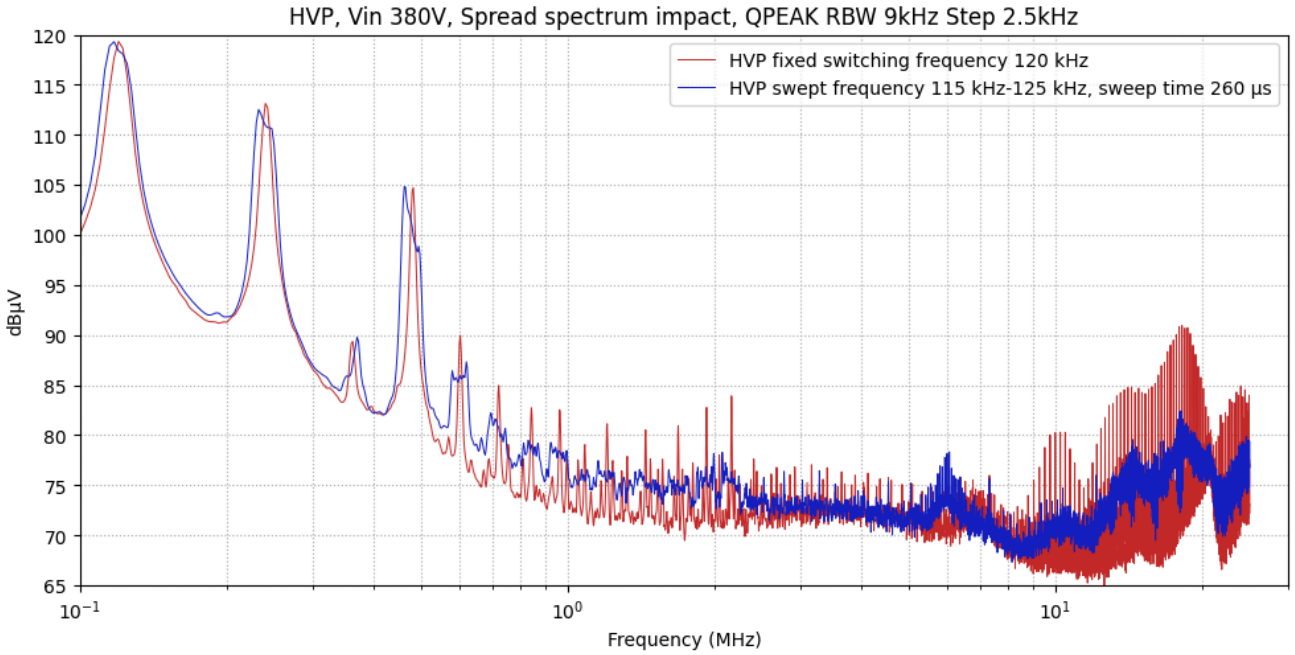
Other investigation

The setup used in the first part and in the annexes is essentially identical. For this section, the setup was disassembled and reassembled, which may introduce minor variations, particularly in the high-frequency region.
To ensure a valid comparison, a new reference measurement was performed with the same configuration, allowing the impact of each subsequent modification to be accurately evaluated.

Frequency sweep (spread spectrum)

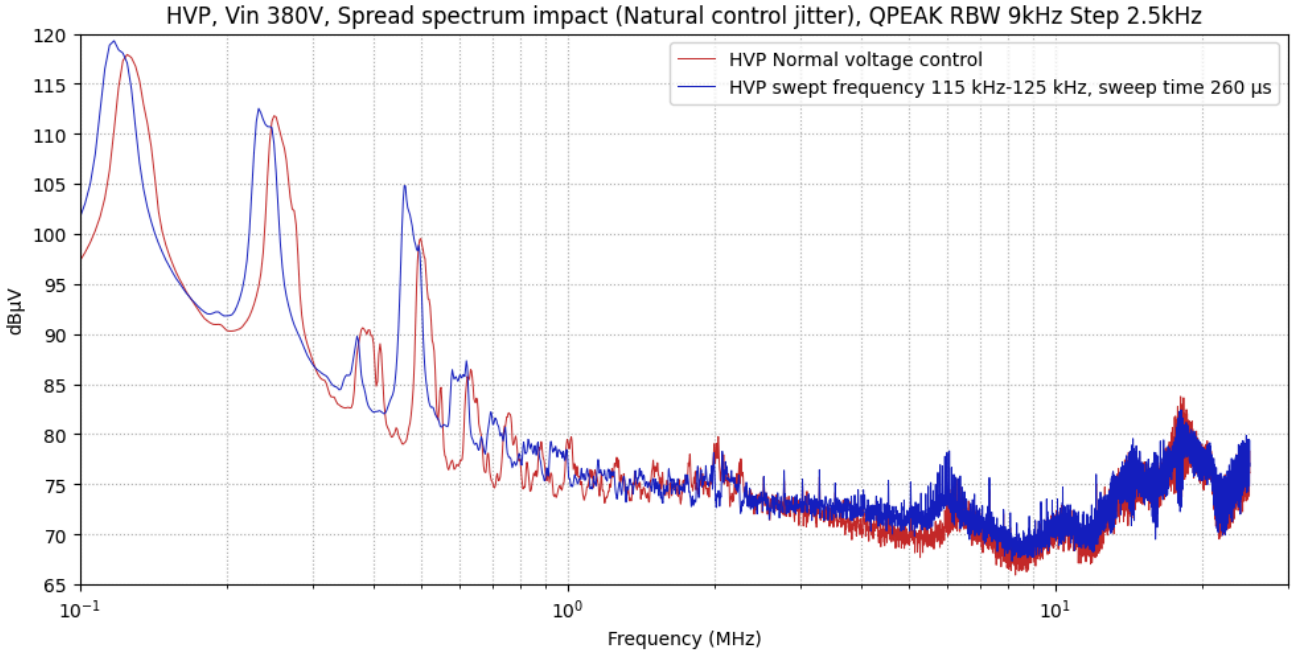
To evaluate the impact of spread-spectrum operation, two control modes are implemented:

- fixed switching frequency of 120 kHz This mode is not representative of a realistic operating condition, but is used to illustrate the effect of a highly stable operating point with a constant switching frequency.
- swept switching frequency from 115 kHz to 125 kHz, with a sweep period of 260 µs This corresponds to a triangular frequency modulation with a 260 µs period and a ±5 kHz deviation around a 120 kHz center frequency.



- Approximately 7 dBµV reduction attributed to the spread-spectrum technique around 2 MHz.
- Approximately 10 dBµV reduction observed around 20 MHz.

It should be noted that almost no reduction is observed on the first harmonic at 120 kHz. This is explained by the modulation amplitude of 10 kHz, which is comparable to the IF filter resolution bandwidth (RBW) of 9 kHz. For higher-order harmonics, the effective frequency deviation increases proportionally (example: 2 × 10 kHz = 20 kHz for the second harmonic), causing the spectral energy to spread beyond the 9 kHz RBW and resulting in measurable attenuation.



- First observation: the nominal voltage control is centered around a frequency slightly offset from 120 kHz, resulting in all red harmonics being shifted toward the heigh-frequency side.
- The improvement due to spread-spectrum operation is limited. This can be attributed to the fundamental instability of the regulation control loop, which introduces a natural frequency

modulation.

In conclusion, an excessively stable control loop in an LLC converter is not favorable from an EMI testing perspective.

Impact of sweep time on spread-spectrum performance

The following Python simulation models three signals with identical amplitudes of ±10 mV and a central frequency of 180 kHz, each with a frequency deviation of ±5 kHz. The distinguishing parameter is the sweep time:

- Signal 1: sweep time = 200 µs (5 kHz modulation rate)
- Signal 2: sweep time = 1 ms (1 kHz modulation rate)
- Signal 3: sweep time = 5 ms (200 Hz modulation rate)

Simulation parameters:

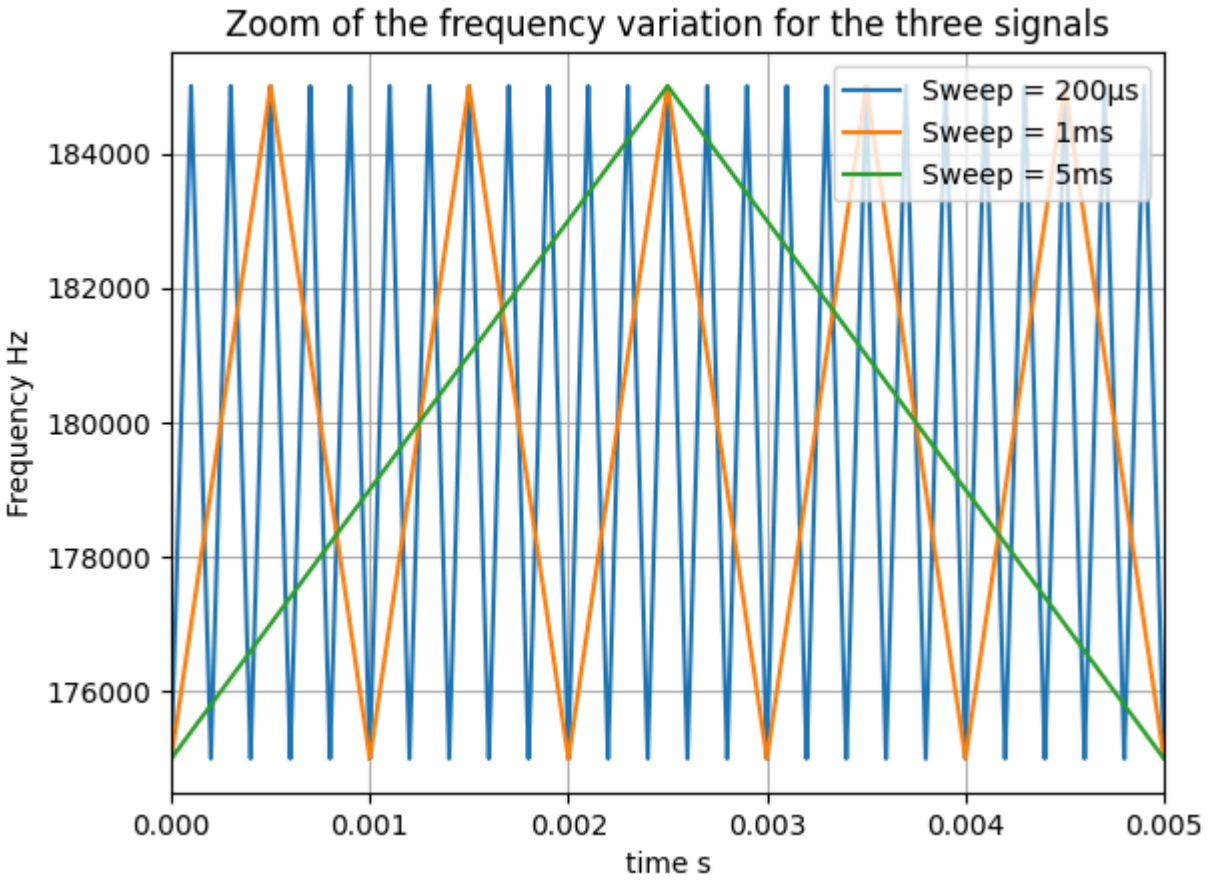
$$\mathrm{Ts} = \frac{1}{10 \times 10^{6}} \qquad = 0.000 \ \ (10\mathrm{Mhz})$$

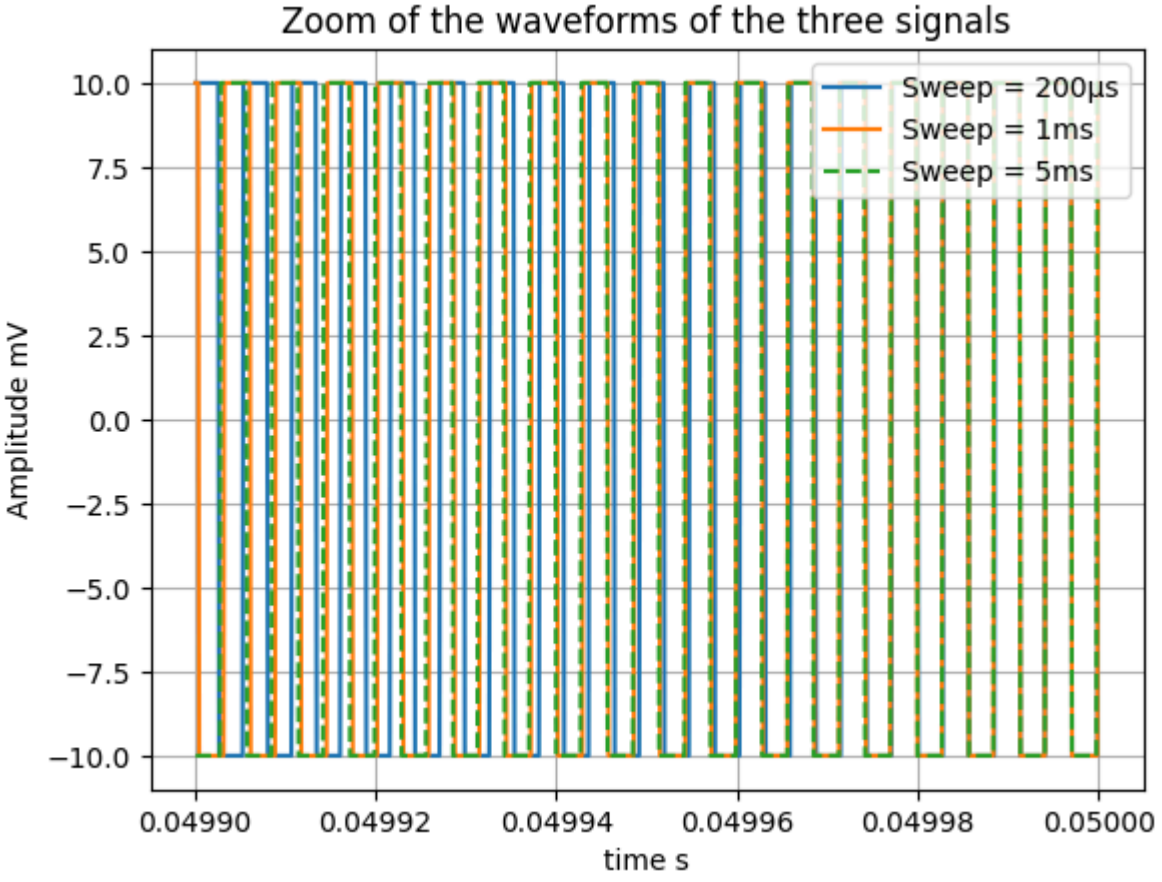
$$\mathrm{MT} = 0.050 \ \ (50\mathrm{ms},\ 20\mathrm{Hz})$$

$$\mathrm{Amp} = 0.010 \ \ (\mathrm{mV})$$

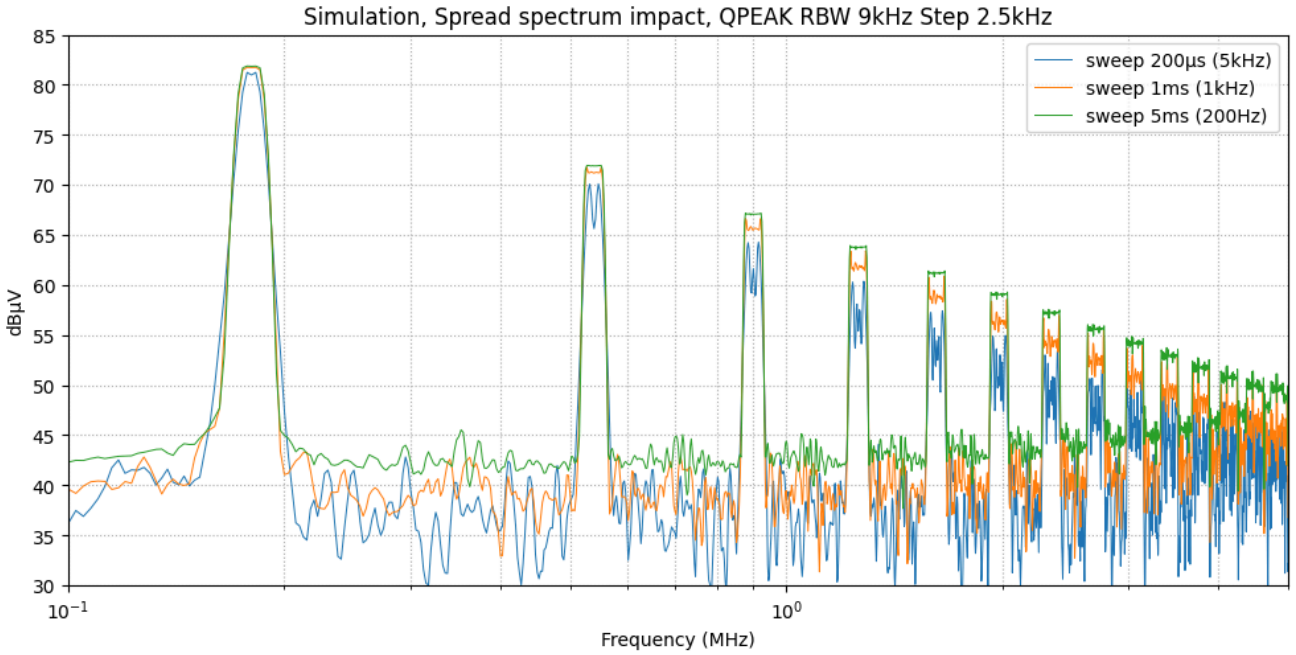
$$\mathrm{Fsw} = 180000.000 \ \ (180\mathrm{kHz})$$

$$\mathrm{deltafreq} = 10000.000 \ \ (10\mathrm{khz})$$





Qpeak results:



We can see that fast sweep time is better

Impact of 220 nF capa in diff mode on the LISN side

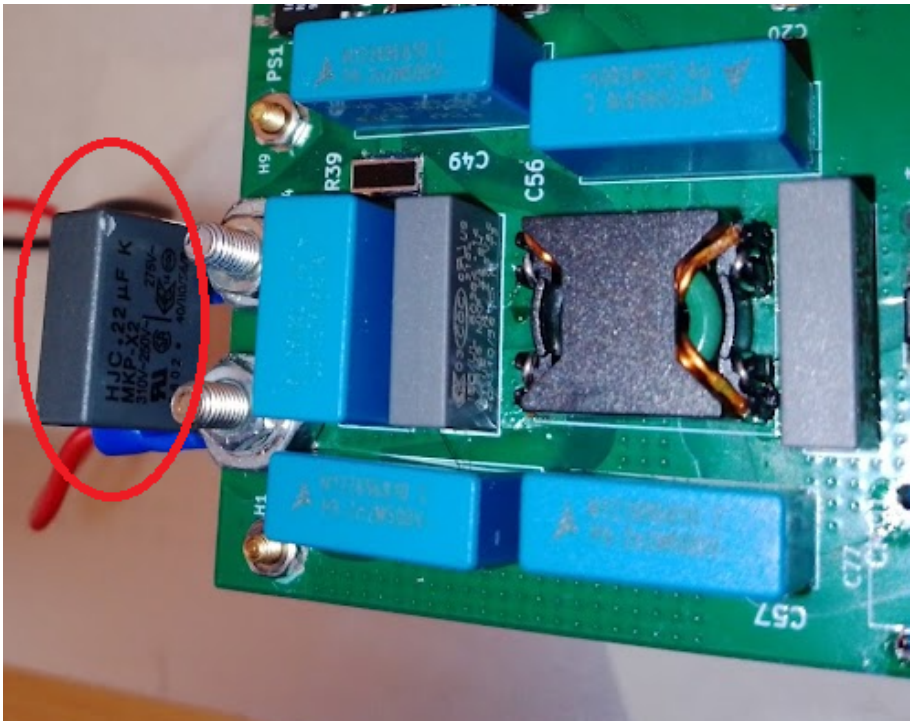
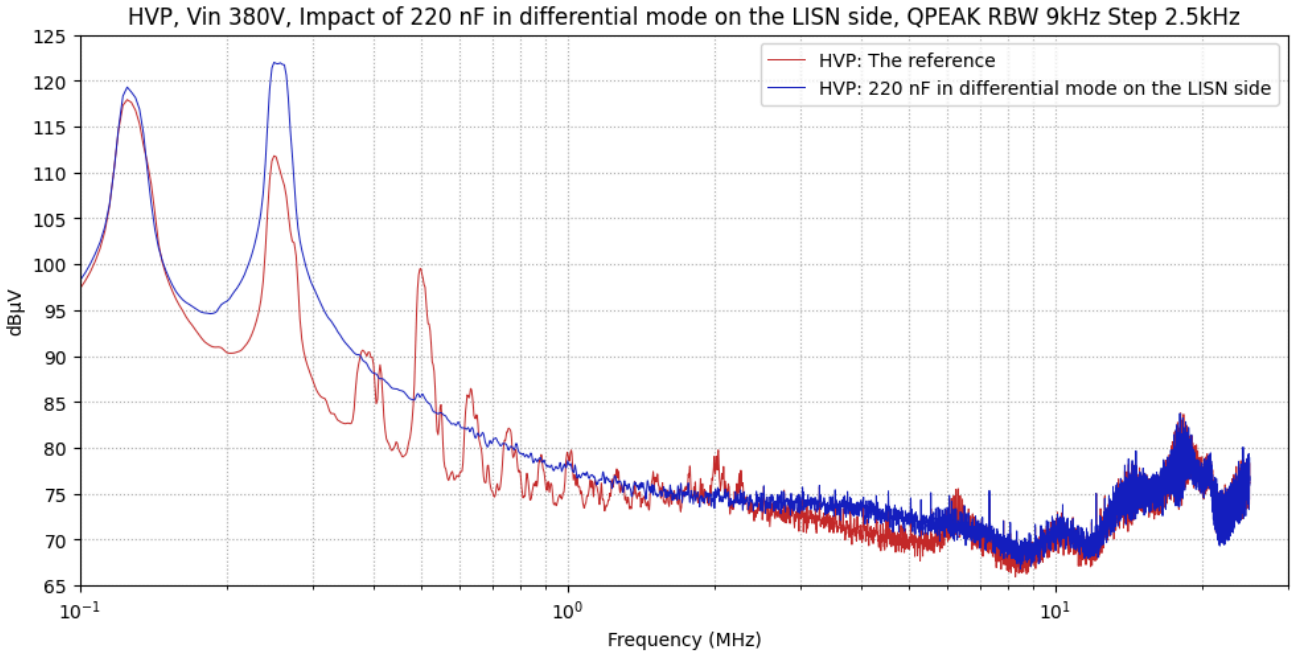


Figure 19: The prototype of a 220 nF capa in diff mode on the LISN side (circled in red)



An improvement is observed in the frequency range from 0.4 MHz to 2 MHz; however, degradation appears at lower frequencies, notably around 240 kHz.

Impact of 1.5 µF capa in diff mode on the LISN side

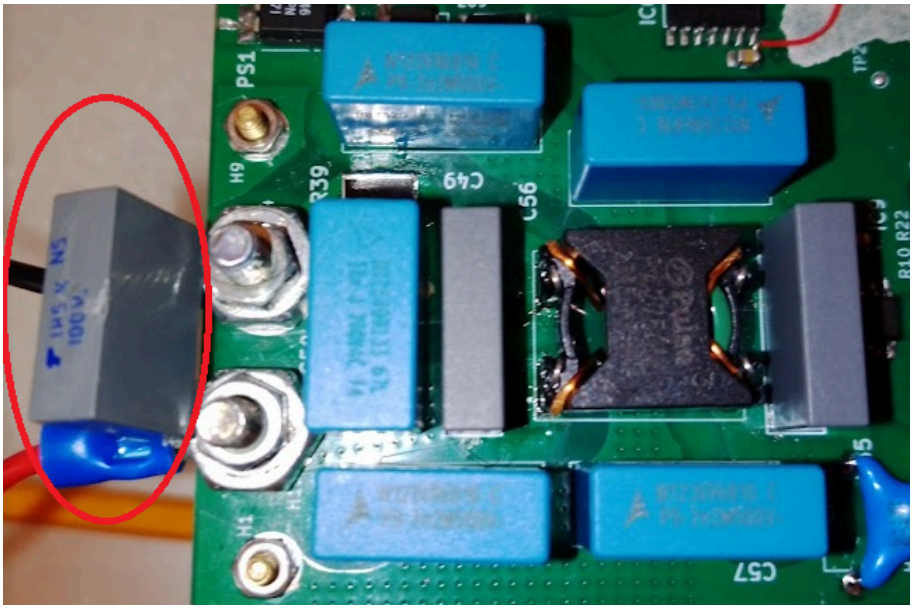
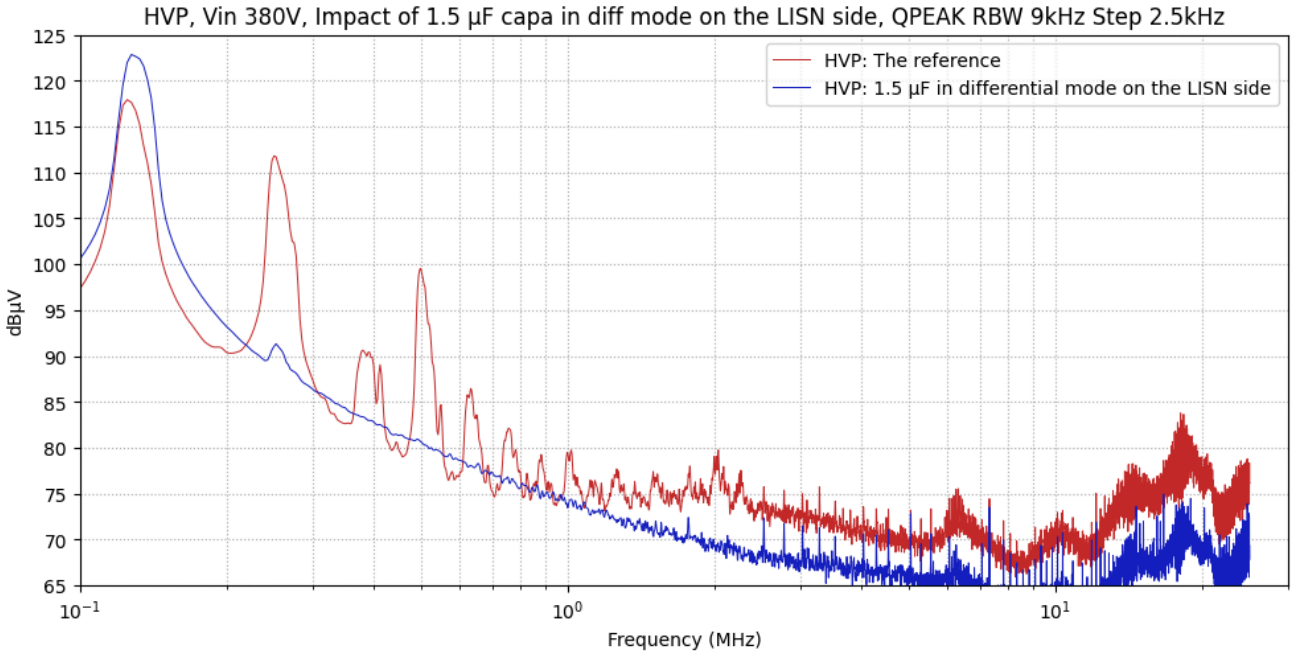


Figure 20: The prototype of a 1.5 µF capa in diff mode on the LISN side (circled in red)



A substantial improvement is observed in the high-frequency range; however, degradation occurs at the first harmonic, located around 120 kHz.

Impact of 100nF capa in common mode on the switchs side

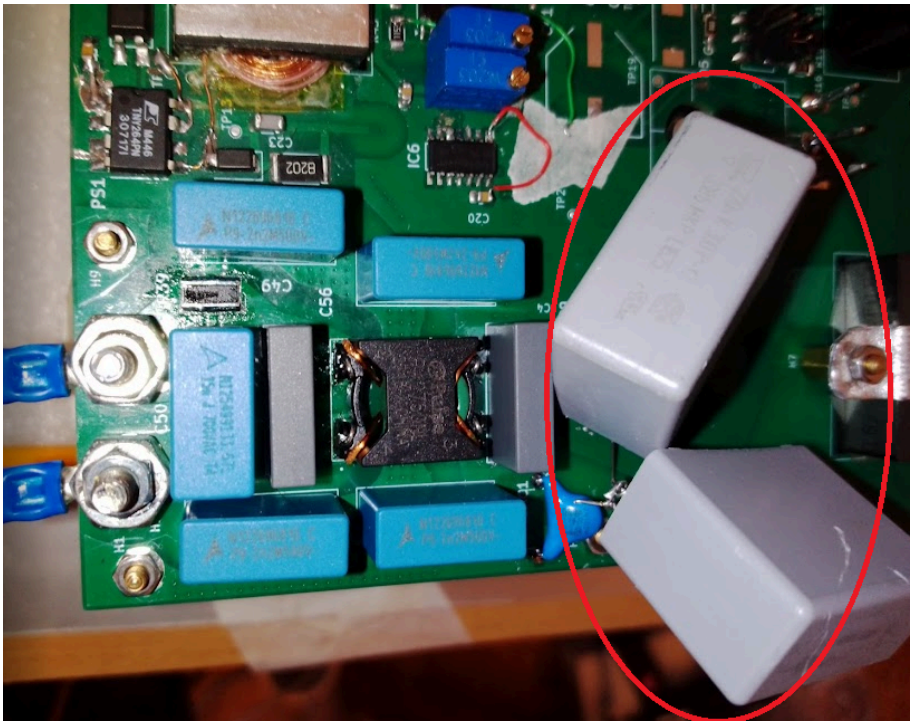
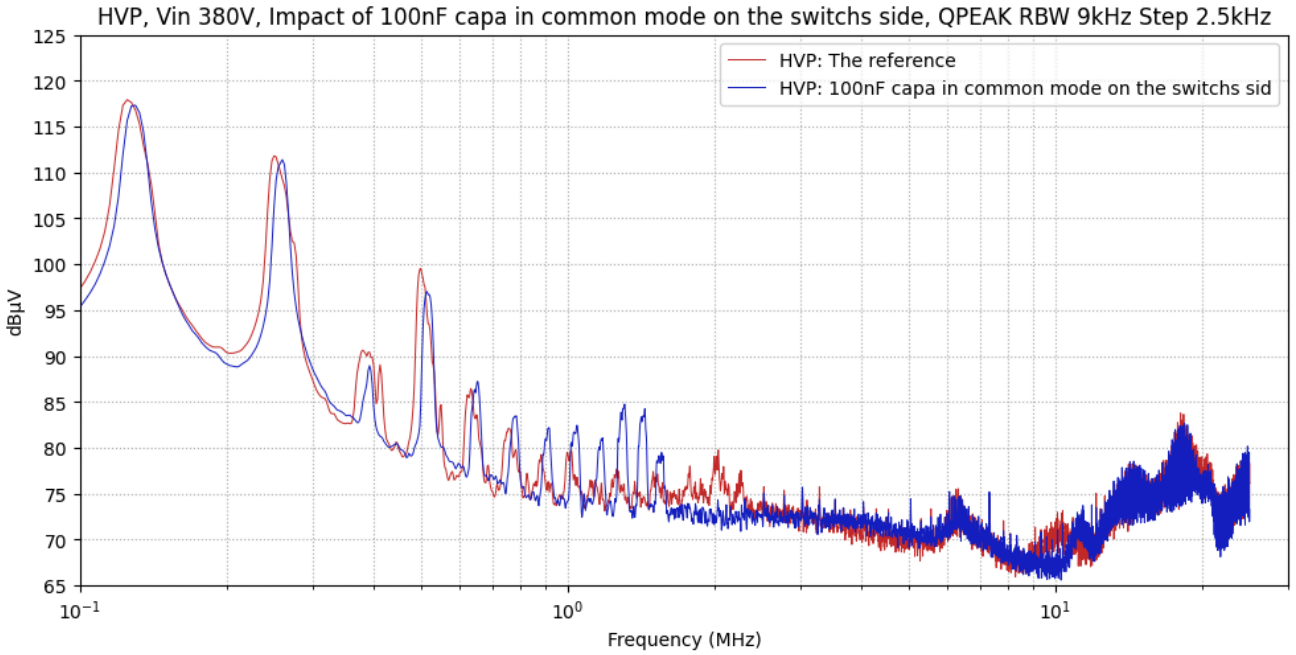
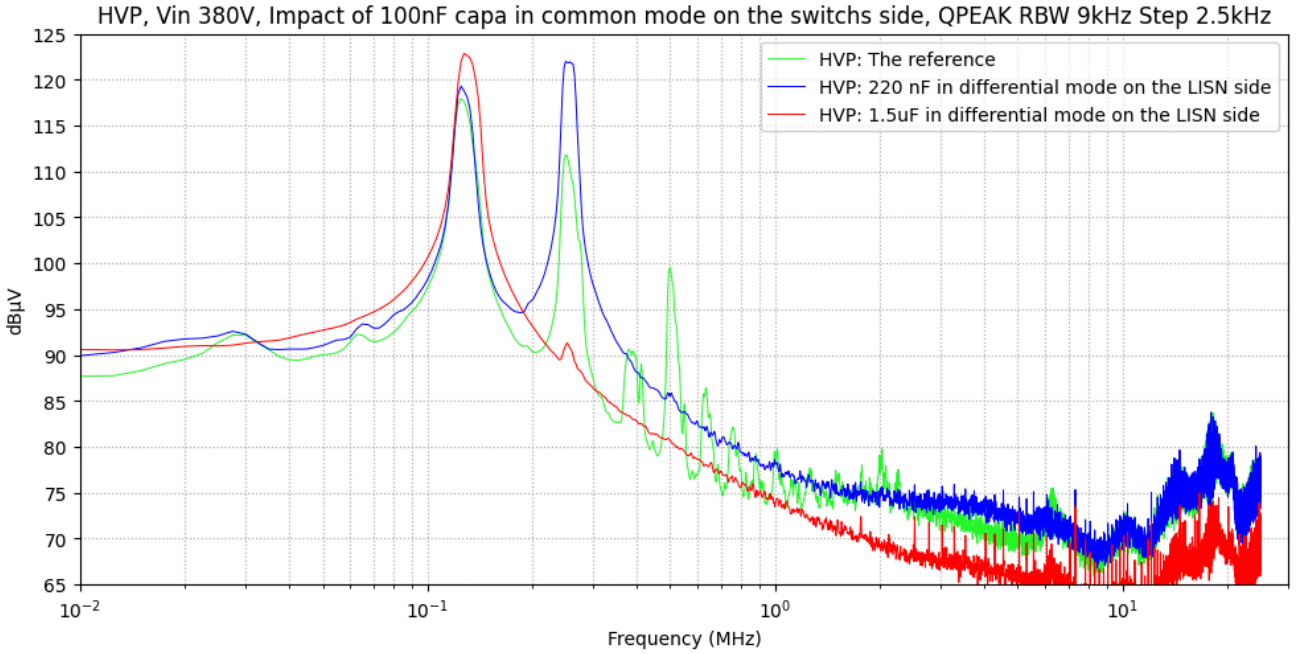


Figure 21: The prototype of a 400V-100nF capa in common mode on the switchs side (circled in red)



Negligible improvement is observed.

Analysis of the significant effect of differential capacitors 220 nF and 1.5 µF



It can be observed that the addition of a differential-mode capacitor shifts the differential-mode resonance toward lower frequencies (left side).

The same behavior is also observed in the simplified differential-mode simulation presented below, where the curves share the same color coding.

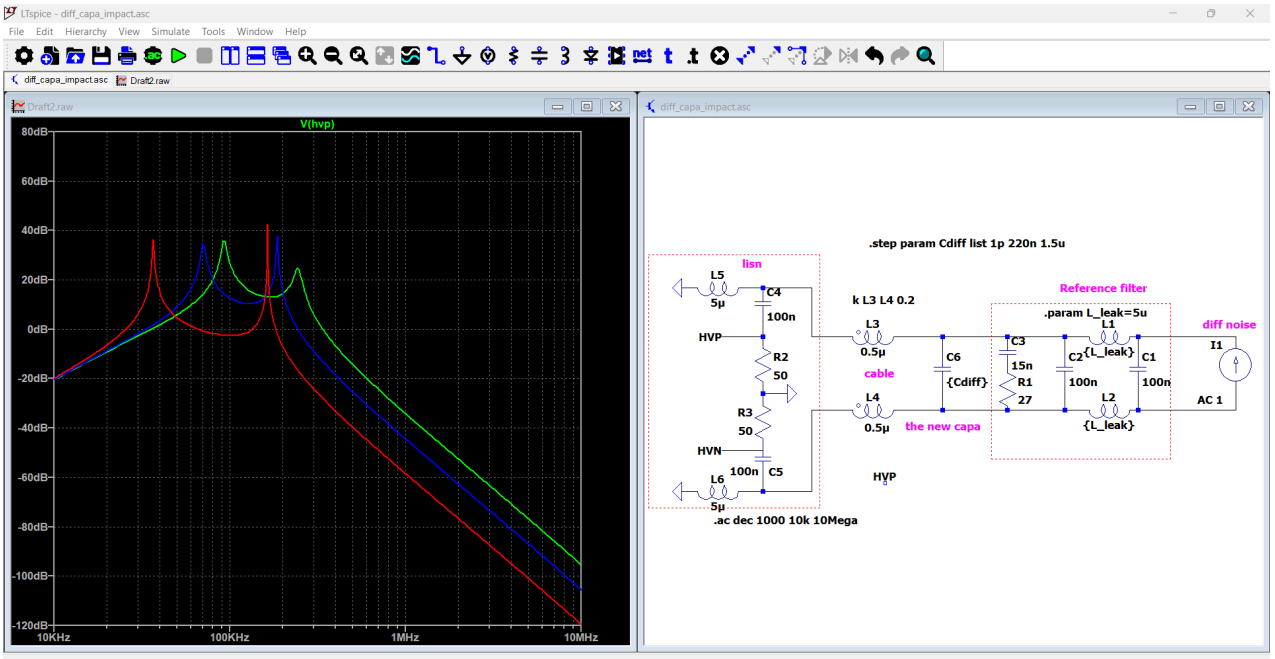


Figure 22: Diff mode capa impact LISN side: Simplified differential-mode simulation

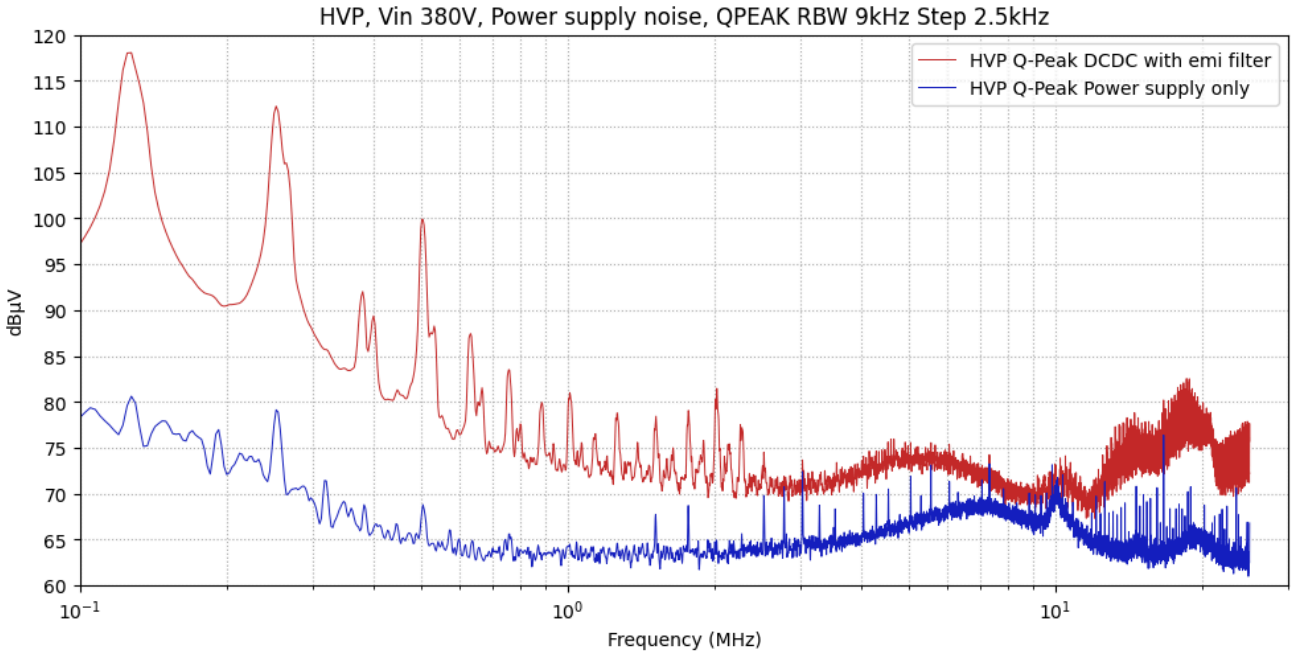
You can found the simulation file in the folder ".\01_Conducted_Emissions_Test\simulations"

Annexes

In this section, you will find additional annex tests that help clarify and support the overall analysis of the conducted EMI measurements.

Main power supply noise

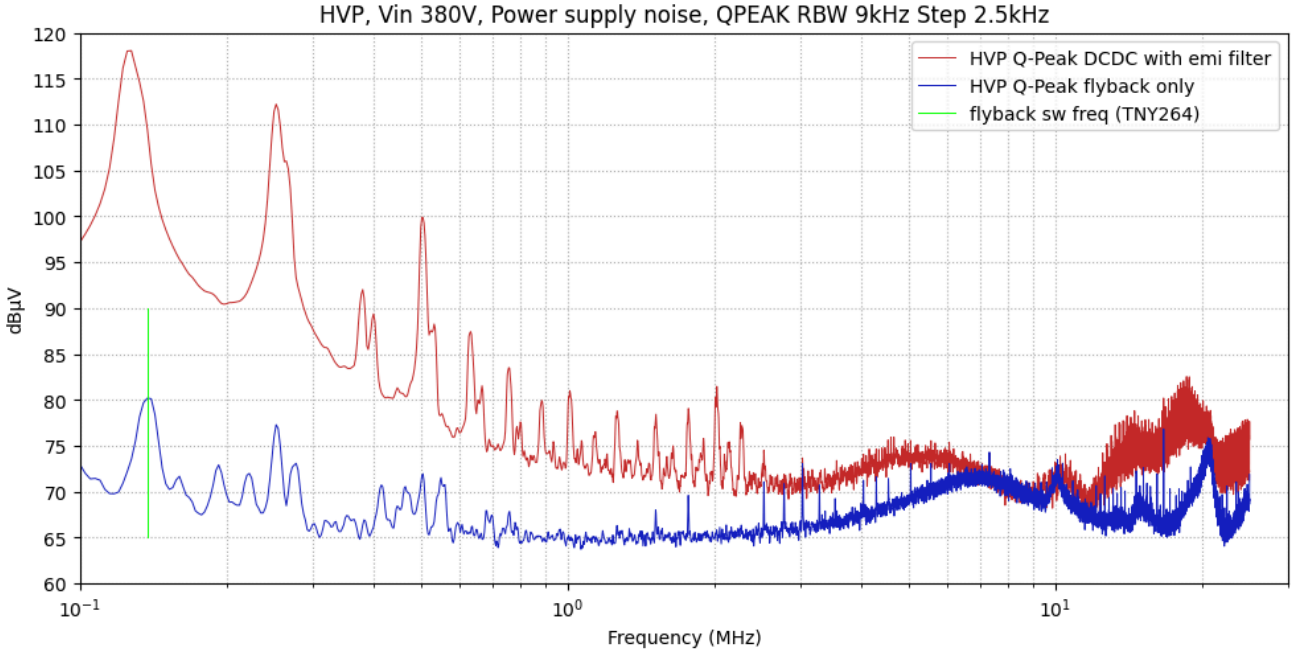
In this test, only the power supply is connected to the LISN, and all wires on the EUT side are removed.
The objective is to evaluate how much noise from the power supply propagates through the LISN.



In this graph, we compare the HVP measurements with and without the DCDC connected. The power-supply noise does not appear to dominate in the 150 kHz to 30 MHz range.
However, adding an output EMI filter between the power supply and the LISN could further reduce this noise and improve the overall result.

FlyBack noise

In this test, the gate-driver jumper is opened to disable DCDC switching, allowing us to measure only the contribution of the flyback circuit.
The fans remain powered and draw approximately 4 W from the flyback



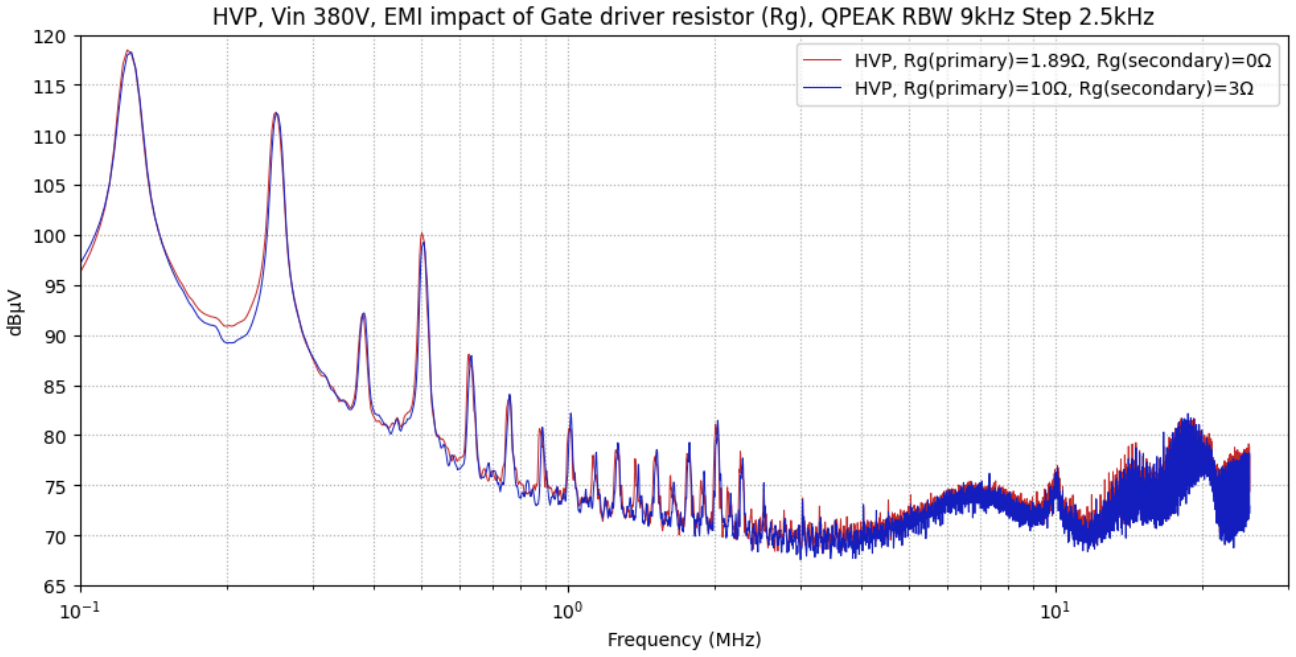
Because the TNY264 controller operates at 132 kHz and includes ±8 kHz frequency jitter for spread-spectrum noise reduction, we expected a noticeable decrease in EMI.

However, the measured improvement is minimal. We confirmed that the flyback is active during this test, yet the results remain far below expectations, indicating that additional checks and deeper investigation are required.

EMI impact of Gate driver resistor (Rg)

In this test, we evaluate the impact of switching speed using two different gate-drive configurations:

- **Configuration 1:**
  - Primary gate-drive resistance: parallel combination of 5.1 Ω and 3 Ω, giving an effective Rg of ***1.89 Ω***
  - Secondary gate-drive resistance: ***0 Ω***
- **Configuration 2:**
  - Primary gate-drive resistance: ***10 Ω***
  - Secondary gate-drive resistance: ***3 Ω***



A slight improvement is observed in the high-frequency range when using higher gate-drive resistors (slower switching), but the effect remains limited.
The impact is smaller than expected, indicating that switching-speed reduction alone may not be the dominant factor in this EMI behaviour.

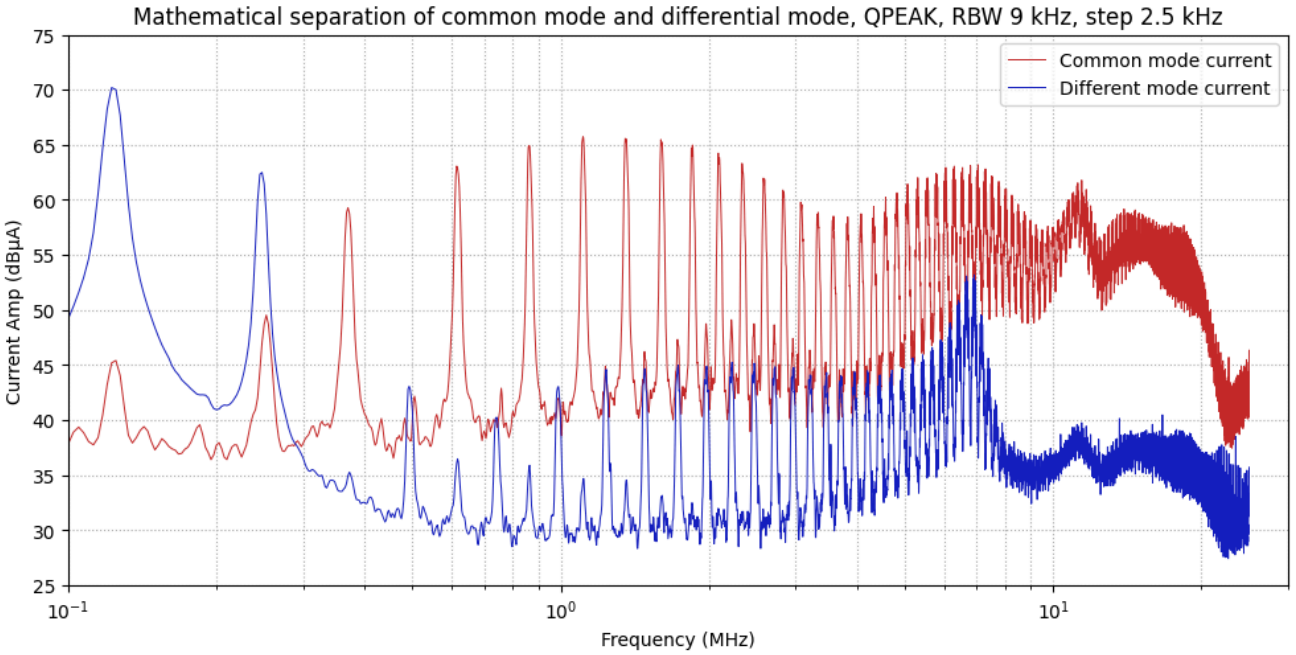
Common-mode and Differential-mode Separation (Math)

In this test, we compare the CT-based method for separating common-mode and differential-mode noise (discussed earlier) with a mathematical approach. In the mathematical method, we measure the voltage on each LISN channel and then compute the corresponding common-mode and differential-mode components.

A start-synchronized acquisition with a stop button is used on the oscilloscope to eliminate timing delays between the two measurement channels. The formulas used to calculate the common-mode and differential-mode currents are shown below.

$$i_{cm} = \frac{\text{Channel}_{Voltage1} + \text{Channel}_{Voltage2}}{R_{Terminal}}$$

$$i_{dm} = \frac{\text{Channel}_{Voltage1} - \text{Channel}_{Voltage2}}{R_{Terminal} \cdot 2}$$



This method is not very robust. With the CT method, the sum and difference of the currents are performed physically, ensuring accurate separation of modes. In contrast, the mathematical approach relies on post-sampling calculations, so even a small timing mismatch between oscilloscope channels can introduce significant errors—especially at high frequencies.

A small ADC-related delay of about 10 ns is enough to shift two synchronised 50 MHz sine waves by up to 180°, meaning the computed difference can vary from 0 to 2×Amplitude. This illustrates how even tiny channel-to-channel timing errors can create large calculation errors at high frequencies.